An analytical solution for the elastic response to surface loads imposed on a layered, transversely isotropic and self-gravitating Earth

E. Pan,[1] J.Y. Chen,[2] M. Bevis,[3] A. Bordoni,[4] V.R. Barletta[3] and A. Molavi Tabrizi[1]

[1]*Department of Civil Engineering, University of Akron, Akron, OH 44325-3905, USA. E-mail:* pan2@uakron.edu
[2]*School of Mechanical Engineering, Zhengzhou University, Henan 450001, China*
[3]*School of Earth Sciences, Ohio State University, Columbus, OH 43210, USA*
[4]*DTU COMPUTE, Kgs. Lyngby, Denmark*

SUMMARY

We present an analytical solution for the elastic deformation of an elastic, transversely isotropic, layered and self-gravitating Earth by surface loads. We first introduce the vector spherical harmonics to express the physical quantities in the layered Earth. This reduces the governing equations to a linear system of equations for the expansion coefficients. We then solve for the expansion coefficients analytically under the assumption (i.e. approximation) that in the mantle, the density in each layer varies as $1/r$ (where r is the radial coordinate) while the gravity is constant and that in the core the gravity in each layer varies linearly in r with constant density. These approximations dramatically simplify the subsequent mathematical analysis and render closed-form expressions for the expansion coefficients. We implement our solution in a MATLAB code and perform a benchmark which shows both the correctness of our solution and the implementation. We also calculate the load Love numbers (LLNs) of the PREM Earth for different degrees of the Legendre function for both isotropic and transversely isotropic, layered mantles with different core models, demonstrating for the first time the effect of Earth anisotropy on the LLNs.

Key words: Composition of the planets; Elasticity and anelasticity; Dynamics: gravity and tectonics; Mechanics, theory and modelling; Planetary interiors.

1 INTRODUCTION

Deformation of the Earth under various surface loadings is a much discussed but rather challenging topic (Farrell 1972; Spada *et al.* 2011; Wang *et al.* 2012). The difficulties include accounting for the (approximately) spherical shape of the Earth, its internal material and mechanical structure, and self-gravitation. In this work, we focus on Earth's instantaneous elastic response to surface loading, and we defer consideration of viscoelastic deformation to a future study.

Green's function methods provide a powerful approach to a wide variety of engineering and scientific problems (for a review, see e.g. Pan & Chen 2015). In Earth science for instance, in order to solve the general surface loading problem associated with a layered, self-gravitating, spherical Earth, we need only to find the Green's functions corresponding to a concentrated point force applied on the surface of the Earth. Solutions of such Green's functions are called the load Love numbers (LLNs) when expanding the solution in a spherical coordinate system.

So far the surface loading problem for a layered elastic (or viscoelastic) and self-gravitating Earth has been solved analytically only for the case of an incompressible Earth, while the compressible case is usually solved numerically (e.g. Farrell 1972; Guo *et al.* 2004; Cambiotti *et al.* 2009; Nield *et al.* 2014), except for the work by Gilbert & Backus (1968) where the gravity in each layer of the Earth was characterized as a linear function of the radial coordinate r. Comparing to those derived numerically, analytical Green's functions of the surface-loading or the LLNs are computationally faster.

We present, in this paper, a new analytical method to derive the Green's functions in response to a point load on the surface of a spherical, transversely isotropic, layered and self-govrating Earth. We have obtained this analytical solution under the assumption that, in the mantle the density in each layer varies as $1/r$ and the gravity is constant, and that in the core the gravity in each layer varies linearly in r with constant density. The solution is exact in case of a single layer for this specific Darwin's law-type density profile. The solution is instead only an

approximation in case of a layered Earth. However, we show that by increasing the number of layers, the solution tends exactly to the correct one, differently from what happens with the Gilbert & Backus (1968) solution.

This paper is organized as follows. In Section 2, we present the governing equations of a transversely isotropic, layered and self-gravitating Earth using the spherical coordinate system. We also recall the definition and main properties of the vector spherical harmonics (VSH). In Section 3, we derive the analytical solution, and its application to the layered mantle in terms of propagator matrices. To achieve our goal, we first derive the equations which govern the expansion coefficients. We then present the analytical solution for the expansion coefficients in the mantle of the Earth under the assumption that, in each layer, the density varies as $1/r$ (where r is the radial coordinate) while the gravity is constant. We finally obtain the propagator matrix and thus the solution in the layered mantle. In Section 4, the analytical solution in the core is derived along with the corresponding core–mantle boundary conditions. In the core, we assume that the gravity in each layer varies linearly in r with constant density. Also in this section, different core models are discussed. In Section 5, we define the LLNs. In Section 6, we first validate our LLNs against the benchmarks (Spada *et al.* 2011), estimating the magnitude of the effect of the approximation on the LLN. We then present numerical results of LLNs for five earth models, all based on Dziewonski & Anderson's (1981) Preliminary Reference Earth Model (PREM). Our earth models clearly demonstrate that with only 56 layers in the mantle and 26 layers in the core, we can achieve a relative error of less than 1 per cent on the density and gravity distributions against the PREM model. Conclusions are drawn in Section 7. Seven appendices are provided for the readers' convenience.

2 GOVERNING EQUATIONS AND VECTOR SPHERICAL HARMONICS

We assume a spherically layered Earth with each layer satisfying the following governing equations (e.g. Farrell 1972; Wu & Peltier 1982)

$$\sigma_{ji,j} - (\rho g u_r)_{,i} - \rho \psi_{,i} + g(\rho u_j)_{,j} \delta_{ir} + f_i = 0; \quad \psi_{,jj} + 4\pi G(\rho u_j)_{,j} = 0. \tag{1}$$

In eq. (1), repeated indices take the summation over the spherical coordinates (r, θ, ϕ) and an index following the subscript comma indicates the derivative in the coordinate direction, G is the universal constant of gravitation, δ the Kronecker delta, σ_{ji} the stresses, ρ and g are the density and gravitational acceleration, f_i the body forces (per unit volume), u_i the displacements, and ψ is the perturbed gravitational potential (which may include the tidal body-force, surface load and deformation potentials) with its negative gradient being the perturbed gravity. This sign convention is the same as in Farrell (1972) and Wu & Peltier (1982), but opposite to that in Takeuchi & Saito (1972) and Sun (1992).

Strain (tensor ε_{ij}) and displacement relations in spherical coordinates are

$$\varepsilon_{rr} = u_{r,r}; \quad \varepsilon_{\theta\theta} = \frac{u_{\theta,\theta} + u_r}{r}; \quad \varepsilon_{\phi\phi} = \frac{u_{\phi,\phi}}{r \sin\theta} + \frac{u_\theta \cot\theta + u_r}{r}$$

$$2\varepsilon_{r\theta} = u_{\theta,r} + \frac{u_{r,\theta} - u_\theta}{r}; \quad 2\varepsilon_{r\phi} = u_{\phi,r} + \frac{u_{r,\phi}}{r \sin\theta} - \frac{u_\phi}{r}$$

$$2\varepsilon_{\theta\phi} = \frac{u_{\phi,\theta} - u_\phi \cot\theta}{r} + \frac{u_{\theta,\phi}}{r \sin\theta}. \tag{2}$$

We also need the relation between the potential and its gradient which are coupled with the elastic displacements. We define it as the 'generalized flux' below

$$q = \psi_{,r} + 4\pi G \rho u_r + \frac{n+1}{r} \psi, \tag{3}$$

where n is the degree in the VSH defined below.

Instead of making the conventional assumption that the mantle is isotropic, we assume that the mantle is anisotropic but with a specific axis of symmetry. This particular form of anisotropic medium is known as transversely isotropic in the literature (Anderson 1961). For the spherical Earth, transverse isotropy means that the material axis of symmetry is along the radial direction and that the material property on any sphere of given radius is isotropic. This allows us to analytically solve the equations including the anisotropic mantle layers given in Dziewonski & Anderson (1981).

The Hooke's law for each of the spherical mantle layer which is transversely isotropic with r-direction being its material axis of symmetry is (Anderson 1961; Chen *et al.* 2015)

$$\sigma_{rr} = c_{33}\varepsilon_{rr} + c_{13}\varepsilon_{\theta\theta} + c_{13}\varepsilon_{\phi\phi}$$

$$\sigma_{\theta\theta} = c_{13}\varepsilon_{rr} + c_{11}\varepsilon_{\theta\theta} + c_{12}\varepsilon_{\phi\phi}$$

$$\sigma_{\phi\phi} = c_{13}\varepsilon_{rr} + c_{12}\varepsilon_{\theta\theta} + c_{11}\varepsilon_{\phi\phi}$$

$$\sigma_{\theta r} = 2c_{44}\varepsilon_{\theta r}; \quad \sigma_{\phi r} = 2c_{44}\varepsilon_{\phi r}; \quad \sigma_{\theta\phi} = 2c_{66}\varepsilon_{\theta\phi}, \tag{4}$$

where c_{ij} are the elastic constants with $c_{66} = (c_{11} - c_{12})/2$.

For the isotropic elastic material, eq. (4) is reduced to

$$c_{11} = c_{33} = \lambda + 2\mu$$

$$c_{12} = c_{13} = \lambda; \quad c_{44} = c_{66} = \mu, \tag{5}$$

where λ and μ are the two Lame's elastic constants.

In the following, we will solve the equations under the general anisotropic formulation (4). The results for the usual isotropic case are obtained automatically when eq. (5) is satisfied.

The interface conditions between any two adjacent layers (with superscript plus and subscript minus signs for them) in the mantle are

$$[u_i]_-^+ = 0; \quad [\sigma_{ri}]_-^+ = 0; \quad i = r, \theta, \phi$$

$$[\psi]_-^+ = 0; \quad [q]_-^+ = 0. \tag{6}$$

The surface condition and the condition at the core–mantle boundary will be discussed later in the paper.

To solve the loading problem we employ the VSH in terms of the spherical coordinates. The VSH is defined as (Ulitko 1979; Chen *et al.* 2015)

$$\boldsymbol{L}(\theta, \phi; n, m) = \boldsymbol{e}_r S(\theta, \phi; n, m)$$

$$\boldsymbol{M}(\theta, \phi; n, m) = r\nabla S = \left(\boldsymbol{e}_\theta \partial_\theta + \boldsymbol{e}_\phi \frac{\partial_\phi}{\sin\theta}\right) S(\theta, \phi; n, m)$$

$$\boldsymbol{N}(\theta, \phi; n, m) = r\nabla \times (\boldsymbol{e}_r S) = \left(\boldsymbol{e}_\theta \frac{\partial_\phi}{\sin\theta} - \boldsymbol{e}_\phi \partial_\theta\right) S(\theta, \phi; n, m), \tag{7}$$

where $\boldsymbol{e}_r$, $\boldsymbol{e}_\theta$ and $\boldsymbol{e}_\phi$ are the unit vectors, respectively, along r-, θ- and ϕ-directions, and S is the normalized spherical harmonic function. It should be noted that while $\boldsymbol{L}$ and $\boldsymbol{M}$ represent the spheroidal deformation (called *LM*-type deformation), $\boldsymbol{N}$ represents the toroidal deformation (called *N*-type deformation). Some basic properties of this spherical harmonic function S and the VSH are provided in Appendix A for easy reference.

Since the system (7) is orthonormal, we can expand any vector, such as the displacement $\boldsymbol{u}$, radial traction $\boldsymbol{t}$, as well as the scalar gravitational potential ψ, and flux q in terms of the system as

$$\boldsymbol{u}(r, \theta, \phi) = \sum_{n=0}^{\infty}\sum_{m=-n}^{n} [U_L(r)\boldsymbol{L}(\theta, \phi) + U_M(r)\boldsymbol{M}(\theta, \phi) + U_N(r)\boldsymbol{N}(\theta, \phi)]$$

$$\boldsymbol{t}(r, \theta, \phi) \equiv \sigma_{rr}\boldsymbol{e}_r + \sigma_{r\theta}\boldsymbol{e}_\theta + \sigma_{r\phi}\boldsymbol{e}_\phi$$

$$= \sum_{n=0}^{\infty}\sum_{m=-n}^{n} [T_L(r)\boldsymbol{L}(\theta, \phi) + T_M(r)\boldsymbol{M}(\theta, \phi) + T_N(r)\boldsymbol{N}(\theta, \phi)]$$

$$\boldsymbol{f}(r, \theta, \phi) = \sum_{n=0}^{\infty}\sum_{m=-n}^{n} [F_L(r)\boldsymbol{L}(\theta, \phi) + F_M(r)\boldsymbol{M}(\theta, \phi) + F_N(r)\boldsymbol{N}(\theta, \phi)]$$

$$\psi(r, \theta, \phi) = \sum_{n=0}^{\infty}\sum_{m=-n}^{n} \Phi(r)S(\theta, \phi)$$

$$q(r, \theta, \phi) = \sum_{n=0}^{\infty}\sum_{m=-n}^{n} Q(r)S(\theta, \phi). \tag{8}$$

We remark that the expansion coefficients on the right-hand side of eq. (8) depend on the coordinate r as well as on degree n and order m (as the vector and scalar spherical harmonics do). In the following discussion, we concentrate on the case where $n \geq 1$. The special case of $n = 0$ (spherically symmetric deformation involving only vector function $\boldsymbol{L}$) is presented in Appendix D.

3 ANALYTICAL SOLUTIONS FOR THE MANTLE

3.1 Equations for the expansion coefficients

We first substitute the expansion expressions for the traction and flux into eqs (3) and (4), and compare the expansion coefficients on both sides of the equations. This gives us, for $n \geq 1$,

$$T_L = 2c_{13}\frac{U_L}{r} + c_{33}U_L' - n(n+1)c_{13}\frac{U_M}{r} \tag{9a}$$

$$T_M = c_{44}\left(U_M' + \frac{U_L - U_M}{r}\right)$$ (9b)

$$Q = \Phi' + 4\pi G\rho U_L + \frac{n+1}{r}\Phi$$ (9c)

$$T_N = c_{44}\left(U_N' - \frac{U_N}{r}\right),$$ (9d)

where a 'prime' denotes the derivative with respect to the radial coordinate (radius) r. Other four equations for the expansion coefficients can be found from eq. (1) as,

$$T_L' - n(n+1)\frac{T_M}{r} + 2\frac{T_L}{r} - 2c_{13}\frac{U_L'}{r} - \frac{2(c_{11}+c_{12})U_L}{r^2} + \frac{(c_{11}+c_{12})n(n+1)U_M}{r^2} + \rho g\left[\frac{2U_L}{r} - \frac{n(n+1)U_M}{r}\right]$$

$$- \rho\left[4\pi G\rho - \frac{2g}{r}\right]U_L - \rho\Phi' = -F_L$$ (10a)

$$T_M' + c_{13}\frac{U_L'}{r} + \frac{(c_{11}+c_{12})U_L}{r^2} - c_{12}n(n+1)\frac{U_M}{r^2} + 3\frac{T_M}{r} + \frac{2c_{66}[1-n(n+1)]U_M}{r^2} - \rho g\frac{U_L}{r} - \rho\frac{\Phi}{r} = -F_M$$ (10b)

$$\frac{2}{r}\Phi' - \frac{n(n+1)}{r^2}\Phi + \frac{(n+1)}{r^2}\Phi - \frac{(n+1)}{r}\Phi' + Q' + 4\pi G\rho\left[\frac{2U_L}{r} - \frac{n(n+1)U_M}{r}\right] = 0$$ (10c)

$$T_N' + 3\frac{T_N}{r} + \frac{2c_{66}[1-n(n+1)/2]U_N}{r^2} = -F_N.$$ (10d)

It is clear from eqs (9) and (10) that the N-type (i.e. toroidal) deformation governed by eqs (9d) and (10d) is independent from the LM-type (i.e. spheroidal) deformation governed by eqs (9a–c) and (10a–c). Furthermore, while the N-type deformation is decoupled from the gravity and is governed by

$$U_N' = \frac{U_N}{r} + T_N/c_{44}$$

$$T_N' = \frac{[n(n+1)-2]c_{66}U_N}{r^2} - 3\frac{T_N}{r} - F_N,$$ (11)

the LM-type deformation is coupled with the gravity and is governed by

$$T_L = 2c_{13}\frac{U_L}{r} + c_{33}U_L' - n(n+1)c_{13}\frac{U_M}{r}$$ (12a)

$$T_M = c_{44}\left(U_M' + \frac{U_L - U_M}{r}\right)$$ (12b)

$$\Phi' + 4\pi G\rho U_L + \frac{(n+1)}{r}\Phi = Q$$ (12c)

$$T_L' - n(n+1)\frac{T_M}{r} + 2\frac{T_L}{r} - 2c_{13}\frac{U_L'}{r} - \frac{2(c_{11}+c_{12})U_L}{r^2} + \frac{(c_{11}+c_{12})n(n+1)U_M}{r^2} + \rho g\left[\frac{4U_L}{r} - \frac{n(n+1)U_M}{r}\right] - 4\pi G\rho^2 - \rho\Phi' = -F_L$$ (12d)

$$T_M' + c_{13}\frac{U_L'}{r} + \frac{(c_{11}+c_{12})U_L}{r^2} - c_{12}n(n+1)\frac{U_M}{r^2} + 3\frac{T_M}{r} + \frac{2c_{66}[1-n(n+1)]U_M}{r^2} - \rho g\frac{U_L}{r} - \rho\frac{\Phi}{r} = -F_M$$ (12e)

$$\frac{1-n}{r}Q - 4\pi G\rho U_L\frac{1-n}{r} + Q' + 4\pi G\rho\left[\frac{2U_L}{r} - \frac{n(n+1)U_M}{r}\right] = 0.$$ (12f)

Eq. (12) can be converted to the following standard first-order differential equations

$$U_L' = -\frac{2c_{13}}{c_{33}}\frac{U_L}{r} + n(n+1)\frac{c_{13}}{c_{33}}\frac{U_M}{r} + \frac{T_L}{c_{33}}$$ (13a)

$$U'_M = -\frac{U_L}{r} + \frac{U_M}{r} + \frac{T_M}{c_{44}}$$
(13b)

$$\Phi' = -4\pi G\rho U_L - \frac{(n+1)}{r}\Phi + Q$$
(13c)

$$T'_L = -\frac{4\rho g U_L}{r} + \frac{2[c_{33}(c_{11}+c_{12}) - 2c_{13}^2]U_L}{c_{33}r^2} + \frac{n(n+1)\rho g U_M}{r} + \frac{[2c_{13}^2 - c_{33}(c_{11}+c_{12})]n(n+1)U_M}{c_{33}r^2}$$
$$+ \frac{2}{r}(c_{13}/c_{33} - 1)T_L + \frac{n(n+1)T_M}{r} - \frac{(n+1)}{r}\rho\Phi + \rho Q - F_L$$
(13d)

$$T'_M = \frac{\rho g U_L}{r} + \frac{[2c_{13}^2 - c_{33}(c_{11}+c_{12})]U_L}{c_{33}r^2} - (c_{11}-c_{12})\frac{U_M}{r^2} + n(n+1)\frac{c_{11}c_{33} - c_{13}^2}{c_{33}}\frac{U_M}{r^2} - \frac{c_{13}T_L}{c_{33}r} - \frac{3T_M}{r} + \frac{\rho\Phi}{r} - F_M$$
(13e)

$$Q' = -4\pi G\rho\frac{(n+1)U_L}{r} + 4\pi G\rho\frac{n(n+1)U_M}{r} + \frac{n-1}{r}Q.$$
(13f)

For the isotropic case, making use of eq. (5), we have

$$U'_L = -\frac{2\lambda}{(\lambda+2\mu)}\frac{U_L}{r} + n(n+1)\frac{\lambda}{(\lambda+2\mu)}\frac{U_M}{r} + \frac{T_L}{(\lambda+2\mu)}$$
(14a)

$$U'_M = -\frac{U_L}{r} + \frac{U_M}{r} + \frac{T_M}{\mu}$$
(14b)

$$\Phi' = -4\pi G\rho U_L - \frac{(n+1)}{r}\Phi + Q$$
(14c)

$$T'_L = -\frac{4\rho g U_L}{r} + \frac{4\mu(3\lambda+2\mu)U_L}{(\lambda+2\mu)r^2} + \frac{n(n+1)\rho g U_M}{r} - \frac{2\mu(3\lambda+2\mu)n(n+1)U_M}{(\lambda+2\mu)r^2}$$
$$- \frac{4\mu}{(\lambda+2\mu)}\frac{T_L}{r} + \frac{n(n+1)T_M}{r} - \frac{(n+1)}{r}\rho\Phi + \rho Q - F_L$$
(14d)

$$T'_M = \frac{\rho g U_L}{r} - \frac{2\mu(3\lambda+2\mu)U_L}{(\lambda+2\mu)r^2} + \frac{2\mu[2n(n+1)(\lambda+\mu) - (\lambda+2\mu)]}{(\lambda+2\mu)}\frac{U_M}{r^2} - \frac{\lambda T_L}{(\lambda+2\mu)r} - \frac{3T_M}{r} + \frac{\rho\Phi}{r} - F_M$$
(14e)

$$Q' = -4\pi G\rho\frac{(n+1)U_L}{r} + 4\pi G\rho\frac{n(n+1)U_M}{r} + \frac{n-1}{r}Q.$$
(14f)

We point out that in deriving eqs (11) and (13), the density and elastic coefficients can all be of arbitrary functions of r and that the gravitational acceleration or gravity g is related to the density by the Newton's gravitational law. We emphasize again that the formulations derived in this section hold only for the mantle materials with degrees $n \geq 1$. We point out also that eqs (14a)–(14f) for the reduced isotropic case are the same first-order system of equations derived and used in the literature (e.g. Wu & Peltier 1982).

3.2 Analytical solutions for the expansion coefficients

While the analytical solution of eq. (11) for the toroidal deformation can be easily found (Watson & Singh 1972), that of eq. (14) for the spheroidal deformation has been always solved numerically, except for the incompressible case (Wu & Peltier 1982) and for the case where the term g/r in the governing equation is assumed to be constant in each layer (Gilbert & Backus 1968). In this paper, we solve eq. (13) analytically by assuming that the density in each layer of the mantle varies as $1/r$, whilst the elastic properties and the gravity g are constant in each layer. As a special case we therefore obtain also the solution for an isotropic mantle material as governed by eq. (14).

Let us first assume that the mantle is composed of p layers, with layer j of the layered Earth is bonded on its top at $r = r_j$ and its bottom at $r = r_{j-1}$ so that the thickness of layer j is $h_j = r_j - r_{j-1}$ (Fig. 1). The bottom surface of the first layer is at $r = r_0 \equiv r_c$, that is the core–mantle boundary of the Earth. The structure of the liquid core will be analysed later on.
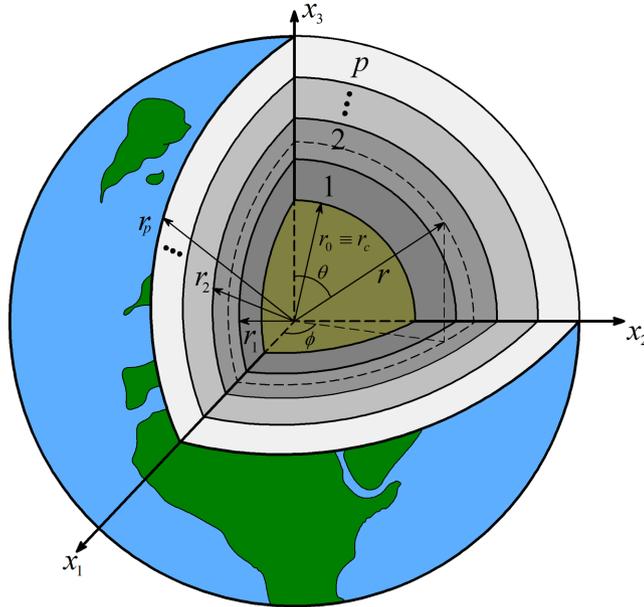
Figure 1. A layered spherical Earth made of p layers in its mantle with an inner (layered) liquid core of radius $r_0 = r_c$. The outer surface of the Earth is located at $r_p = a$. Surface load is applied on $r = a$. In each mantle layer, the density is approximated to vary as $1/r$, and the elastic coefficients as well as the gravity are assumed to be constant.

Within a given layer j, eq. (13) can be solved analytically if we assume that the gravity is constant whilst the density ρ varies as

$$\rho(r) = \bar{\rho}\bar{r}/r. \tag{15}$$

We point out that the density profile of eq. (15) is one of the so-called Darwin's law profiles (see, e.g. Martinec *et al.* 2001). In the present approach we model the Earth as a sort of expansion in a (finite) number of 'Darwinian' layers.

In case of a layered Earth, $\bar{\rho}$ in eq. (15) must be chosen such that the total mass is conserved in each layer. Starting from a reference model with constant density layers and choosing $\bar{\rho}$ as the volume-average density of layer j, then $\bar{r}$ is determined by

$$\bar{r} = \frac{2(r_j^3 - r_{j-1}^3)}{3(r_j^2 - r_{j-1}^2)}. \tag{16}$$

Eq. (16) ensures that the mass is conserved in the layer and as such, $\bar{r}$ is, in general, different from the geometric mean of layer j.

It is noted, however, that through eq. (15) we introduce artificial discontinuities in the density profile between the adjacent layers. This is part of the price we pay to be able to have an analytic solution.

For the given density distribution one can find the gravity $g(r)$ in each layer using Newton's gravitational law.

$$g(r) = \frac{4\pi G}{r^2} \int_0^r \rho(s)s^2 \mathrm{d}s. \tag{17}$$

Note that, according to eq. (17), in case of a pure Darwin's law profile like eq. (15), g is constant. Therefore the solution is exact in the case of a single layer. This is not true anymore in a layered Earth. However, to be able to use this solution in a layered mantle, we have also to assume that g is constant within each layer. This introduces of course an error in the model, and the solution will depart from the correct one. We will estimate this discrepancy in the section devoted to the numerical results, where we will also show that by tuning the number of density layers, this error can be made arbitrarily small. As a side comment, we emphasize that for the PREM model, the constant g assumption is actually not extremely inaccurate since the gravity varies gently within each layer as will be shown later in the numerical section. We further point out that a general and interesting discussion on the density distribution and the corresponding gravity variation can be found in Vermeersen & Mitrovica (2000) and Martinec *et al.* (2001).

Under the assumption of eq. (15) and $g = $ constant, eq. (13) can be converted to the following first-order differential system of equations:

$$U_L' = -\frac{2c_{13}}{c_{33}}\frac{U_L}{r} + n(n+1)\frac{c_{13}}{c_{33}}\frac{U_M}{r} + \frac{T_L}{c_{33}} \tag{18a}$$

$$U_M' = -\frac{U_L}{r} + \frac{U_M}{r} + \frac{T_M}{c_{44}} \tag{18b}$$

$$\Phi' = -\frac{4\pi G \bar{\rho}\bar{r}}{r}U_L - \frac{(n+1)}{r}\Phi + Q \tag{18c}$$

$$T_L' = -\frac{4\bar{\rho}\bar{r}gU_L}{r^2} + \frac{2[c_{33}(c_{11}+c_{12})-2c_{13}^2]U_L}{c_{33}r^2} + \frac{n(n+1)\bar{\rho}\bar{r}gU_M}{r^2} + \frac{[2c_{13}^2-c_{33}(c_{11}+c_{12})]n(n+1)U_M}{c_{33}r^2}$$

$$+ \frac{2}{r}(c_{13}/c_{33}-1)T_L + \frac{n(n+1)T_M}{r} - \frac{(n+1)\bar{\rho}\bar{r}}{r^2}\Phi + \frac{\bar{\rho}\bar{r}}{r}Q - F_L \tag{18d}$$

$$T_M' = \frac{\bar{\rho}\bar{r}gU_L}{r^2} + \frac{[2c_{13}^2-c_{33}(c_{11}+c_{12})]U_L}{c_{33}r^2} - (c_{11}-c_{12})\frac{U_M}{r^2} + n(n+1)\frac{c_{11}c_{33}-c_{13}^2}{c_{33}}\frac{U_M}{r^2} - \frac{c_{13}T_L}{c_{33}r} - \frac{3T_M}{r} + \frac{\bar{\rho}\bar{r}\Phi}{r^2} - F_M \tag{18e}$$

$$Q' = -\frac{(n+1)4\pi G\bar{\rho}\bar{r}U_L}{r^2} + \frac{n(n+1)4\pi G\bar{\rho}\bar{r}U_M}{r^2} + \frac{n-1}{r}Q. \tag{18f}$$

We now seek the solutions to the corresponding homogeneous systems of eqs (11) and (18). Looking at the right-hand sides of these equations, one immediately observes that the radial coordinate r appears in the displacement/potential and traction/flux expansion coefficients with a power that differs by one order, a feature similar to the linear elasticity (e.g. Watson & Singh 1972; Chen *et al.* 2015). Thus, in order to solve these homogeneous systems of equations, we introduce, for a given layer j with interfaces at $r = r_{j-1}$ and r_j ($>r_{j-1}$) the following variable transformation as in Chen *et al.* (2015)

$$r = r_{j-1}e^{\xi} \qquad 0 \le \xi \le \xi_j; \quad \xi_j = \ln(r_j/r_{j-1}). \tag{19}$$

Under this transformation, the homogeneous systems of eqs (11) and (18) with the special r-dependence coefficients are converted to the following ones with constant coefficients

$$\begin{bmatrix} U_N' \\ rT_N' \end{bmatrix} = \begin{bmatrix} 1 & 1/c_{44} \\ -c_{66}[2-n(n+1)] & -3 \end{bmatrix}\begin{bmatrix} U_N \\ rT_N \end{bmatrix} \tag{20a}$$

$$\begin{bmatrix} \boldsymbol{R}_2 & \boldsymbol{0} \\ -\boldsymbol{R}_5 & \boldsymbol{I} \end{bmatrix}\begin{bmatrix} \boldsymbol{U}' \\ r\boldsymbol{T}' \end{bmatrix} = \begin{bmatrix} -\boldsymbol{R}_1 & \boldsymbol{I} \\ \boldsymbol{R}_4 & \boldsymbol{R}_3 \end{bmatrix}\begin{bmatrix} \boldsymbol{U} \\ r\boldsymbol{T} \end{bmatrix}, \tag{20b}$$

where the prime now indicates the derivative with respect to ξ, not with respect to r, and

$$\boldsymbol{U} = \begin{bmatrix} U_L & U_M & \Phi \end{bmatrix}^t; \quad \boldsymbol{T} = \begin{bmatrix} T_L & T_M & Q \end{bmatrix}^t. \tag{21}$$

The elements of the constant matrices $\boldsymbol{R}_i$ in eq. (20b) are listed in Appendix B.

Treating $r(\xi)T_N$ and $r(\xi)\boldsymbol{T}$ as new functions, eq. (20) can be recast into the following first-order differential equations with constant coefficients

$$\begin{bmatrix} U_N' \\ (rT_N)' \end{bmatrix} = [\boldsymbol{B}^N]\begin{bmatrix} U_N \\ rT_N \end{bmatrix} \tag{22a}$$

$$\begin{bmatrix} \boldsymbol{U}' \\ (r\boldsymbol{T})' \end{bmatrix} = [\boldsymbol{B}]\begin{bmatrix} \boldsymbol{U} \\ r\boldsymbol{T} \end{bmatrix}. \tag{22b}$$

In eq. (22),

$$[\boldsymbol{B}^N] = \begin{bmatrix} 1 & 1/c_{44} \\ -c_{66}[2-n(n+1)] & -2 \end{bmatrix} \tag{23a}$$

$$[\boldsymbol{B}] = \begin{bmatrix} \boldsymbol{R}_2^{-1} & \boldsymbol{0} \\ \boldsymbol{R}_5\boldsymbol{R}_2^{-1} & \boldsymbol{I} \end{bmatrix}\begin{bmatrix} -\boldsymbol{R}_1 & \boldsymbol{I} \\ \boldsymbol{R}_4 & \boldsymbol{R}_3 + \boldsymbol{I} \end{bmatrix}. \tag{23b}$$

Notice again that in case of a uniform Earth with Darwin's law profile (i.e. eq. 15), these equations are exact.

3.3. Propagator matrices and solutions in layered mantle

First, since the coefficient matrices in eq. (22) are independent of ξ, we can analytically find their eigenvalues and the corresponding eigenvectors to form the general solutions of eq. (22) inside each layer. In terms of the exponential matrix formalism directly (i.e. Gantmacher 1977), the analytical solution in each layer can be simply expressed as

$$\begin{bmatrix} U_N(\xi) \\ r(\xi)T_N(\xi) \end{bmatrix} = \exp\left(\boldsymbol{B}^N\xi\right) \begin{bmatrix} U_N(0) \\ r\,T_N(0) \end{bmatrix} \tag{24a}$$

$$\begin{bmatrix} \boldsymbol{U}(\xi) \\ r(\xi)\boldsymbol{T}(\xi) \end{bmatrix} = \exp\left(\boldsymbol{B}\xi\right) \begin{bmatrix} \boldsymbol{U}(0) \\ r\,\boldsymbol{T}(0) \end{bmatrix}. \tag{24b}$$

Now, for layer i, with its inner and outer interfaces at $r = r_{i-1}$ and r_i, the expansion coefficients at its interfaces are connected through

$$\begin{bmatrix} U_N(\xi_i) \\ r_i\,T_N(\xi_i) \end{bmatrix} = \exp\left(\boldsymbol{B}_i^N\xi_i\right) \begin{bmatrix} U_N(\xi_{i-1}) \\ r_{i-1}T_N(\xi_{i-1}) \end{bmatrix} \tag{25a}$$

$$\begin{bmatrix} \boldsymbol{U}(\xi_i) \\ r_i\,\boldsymbol{T}(\xi_i) \end{bmatrix} = \exp\left(\boldsymbol{B}_i\xi_i\right) \begin{bmatrix} \boldsymbol{U}(\xi_{i-1}) \\ r_{i-1}\boldsymbol{T}(\xi_{i-1}) \end{bmatrix}. \tag{25b}$$

Making use of the interface continuity conditions (eq. 6) between any adjacent layers, which requires that the expansion coefficients be continuous as

$$[U_L]_-^+ = 0; \quad [U_M]_-^+ = 0; \quad [U_N]_-^+ = 0$$

$$[T_L]_-^+ = 0; \quad [T_M]_-^+ = 0; \quad [T_N]_-^+ = 0$$

$$[\Phi]_-^+ = 0; \quad [Q]_-^+ = 0, \tag{26}$$

we can propagate the solution (25) from the core–mantle boundary $r = r_c$ (r_0) all the way to the surface of the Earth at $r = a$ (r_p). This gives us

$$\begin{bmatrix} U_N(\xi_p) \\ a\,T_N(\xi_p) \end{bmatrix}\Bigg|_{r=a} = \exp\left(\boldsymbol{B}_p^N\xi_p\right)\exp\left(\boldsymbol{B}_{p-1}^N\xi_{p-1}\right)\cdots\exp\left(\boldsymbol{B}_1^N\xi_1\right) \begin{bmatrix} U_N(\xi) \\ r_c\,T_N(\xi) \end{bmatrix}\Bigg|_{r=r_c} \tag{27a}$$

$$\begin{bmatrix} \boldsymbol{U}(\xi_p) \\ a\,\boldsymbol{T}(\xi_p) \end{bmatrix}\Bigg|_{r=a} = \exp\left(\boldsymbol{B}_p\xi_p\right)\exp\left(\boldsymbol{B}_{p-1}\xi_{p-1}\right)\cdots\exp\left(\boldsymbol{B}_1\xi_1\right) \begin{bmatrix} \boldsymbol{U}(\xi) \\ r_c\,\boldsymbol{T}(\xi) \end{bmatrix}\Bigg|_{r=r_c}, \tag{27b}$$

Making use of the interface conditions on the core–mantle boundary at $r = r_c$ and the surface conditions at $r = a$, eq. (27) can be solved for the involved unknowns on both sides. After that, the expansion coefficients at any r-level within any layer can be found by simply employing the propagating relation (24).

We point out again that the formulations derived so far hold only for the mantle of the Earth and for degree $n \geq 1$. We now discuss and derive the solutions in the core.

4 ANALYTICAL SOLUTIONS IN THE CORE ALONG WITH THE CORE-MANTLE BOUNDARY CONDITIONS

This section again is for degree $n \geq 1$. Three core models that have been studied in recent literature will be discussed. A layered core made of m layers over a homogeneous inner core of radius $r = r_0$ is sketched in Fig. 2.

In order to develop our analytic approach, we assume that, in each core layer, the density is constant and gravity is linear in radius as $g = kr$ (Gilbert & Backus 1968). As for the mantle case, these assumptions are consistent with eq. (17) for a single layer, but are instead an approximation to the correct physics when enforced inside each layer. We emphasize that this assumption is to ensure an analytical solution in each layer of the core (see, Gilbert & Backus 1968; Martinec 2000; Cambiotti *et al.* 2009). We further point out that this specific choice of constant density and linear gravity is actually a good approximation. By examining the PREM model, it is apparent that a reasonable model for approximating the layered core is to assume that, in each layer, the gravity is linear in radius as $g = kr$ with constant density (Gilbert & Backus 1968). In any case, the accuracy of the model needs to be compared with the PREM model, as we will discuss in the numerical section. In the following, however, we first turn our attention to the three common core models.
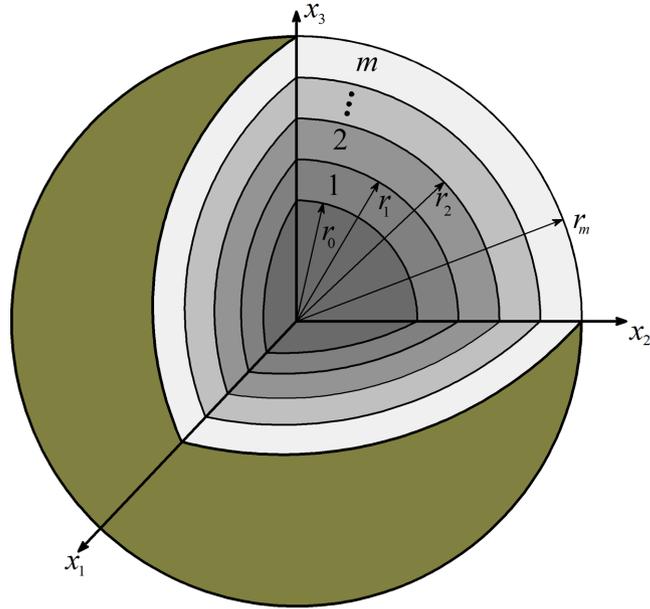
Figure 2. A layered core of the Earth made of m layers over a homogeneous inner core of radius $r = r_0$. Its outer surface is the core–mantle boundary at $r_m = r_c$. In each layer, the gravity is assumed to vary linearly in r with constant density.

4.1 Layered and compressible core

For this model, we follow Saito (1974) and Sun (1992) by introducing the new variable Y which is related to Q, T_L and Φ as

$$Y = Q - \frac{4\pi G}{g} T_L = \Phi' + \left(\frac{n+1}{r} - \frac{4\pi \rho G}{g} \right) \Phi. \tag{28}$$

Then, one can derive the following first-order differential system of equations for Φ and Y as

$$\Phi' = \left(\frac{4\pi \rho G}{g} - \frac{n+1}{r} \right) \Phi + Y$$

$$Y' = \frac{8\pi G \rho (n-1)}{gr} \Phi + \left(\frac{n-1}{r} - \frac{4\pi \rho G}{g} \right) Y, \tag{29}$$

where the density ρ can be any function of r, and the gravity g is related to the density via Newton's gravitational law (17).

To solve this system of equations analytically, we subdivide the core into layers and assume that in each layer the density ρ can be approximated as constant and that the gravity as a linear function $g = kr$. The case of a single layer with constant ρ implies $g = kr$ (eq. 17). So in this case the equations are correct, and the solution is exact. In case of a layered core model, this assumption violates the relation (17) between ρ and g, and therefore the corresponding solutions are not correct any more. However, we will show that the effect introduced by this 'error' can be controlled by choosing the number and thickness of the layers. Now, under the constant density and linear gravity assumption, eq. (29) is reduced to

$$\Phi' = a_{11} \frac{\Phi}{r} + a_{12} Y$$

$$Y' = a_{21} \frac{\Phi}{r^2} + a_{22} \frac{Y}{r}. \tag{30}$$

with the constant coefficients a_{ij} being

$$a_{11} = 4\pi G\rho / k - (n+1); \quad a_{12} = 1$$

$$a_{21} = 8\pi G\rho (n-1)/k; \quad a_{22} = (n-1) - 4\pi G\rho / k. \tag{31}$$

It should be remarked that the structure of eq. (30) can be also achieved by assuming that, in each core layer, the density ρ follows $1/r$ and the gravity g is constant (excluding the innermost layer of the core where one can assume a constant density with a linear gravity, for example Wu & Peltier 1982). However, the first choice is more natural, since the PREM core model indicates that a linear gravity is a better approximation to the gravity distributions in the core than the constant gravity approximation.

Similar to the first-order differential equations governing the *N*-type deformation (eqs 20a and 24a), eq. (30) has an analytical solution in each given layer and thus the following propagating relation in terms of the transformed variable ξ

$$
\begin{bmatrix} \Phi(\xi) \\ r(\xi)Y(\xi) \end{bmatrix} = \exp(A\xi) \begin{bmatrix} \Phi(0) \\ rY(0) \end{bmatrix},
\tag{32}
$$

where

$$
[A] = \begin{bmatrix} a_{11} & a_{12} \\ a_{21} & a_{22}+1 \end{bmatrix}.
\tag{33}
$$

In the innermost core layer with a small radius $r \leq r_0$, eq. (29) has the following solution,

$$
\begin{bmatrix} \Phi \\ rY \end{bmatrix} = \begin{bmatrix} r^n \\ 2(n-1)r^n \end{bmatrix}.
\tag{34}
$$

Thus, we can propagate this solution from $r = r_0$ to the core-mantle boundary at $r = r_c$ to obtain

$$
\begin{bmatrix} \Phi(\xi) \\ r_cY(\xi) \end{bmatrix}\Big|_{r=r_c} = \exp(A_m\xi_m)\exp(A_{m-1}\xi_{m-1})\cdots\exp(A_1\xi_1) \begin{bmatrix} r_0^n \\ 2(n-1)r_0^n \end{bmatrix}.
\tag{35}
$$

Then the physical quantities on the core side of the core-mantle boundary can be transferred to the mantle side using (Saito 1974; Sun 1992)

$$
\begin{bmatrix} U(\xi) \\ r_cT(\xi) \end{bmatrix}\Big|_{r_c} = [B_c] \begin{bmatrix} c_1 \\ c_2 \\ c_3 \end{bmatrix},
\tag{36}
$$

where c_i ($i = 1, 2, 3$) are the three unknown coefficients and B_c is the core–mantle matrix given as

$$
[B_c] = \begin{bmatrix} 0 & 0 & 1 \\ 0 & 1 & 0 \\ \Phi(r_c) & 0 & 0 \\ r_c\rho(r_c)\Phi(r_c) & 0 & r_c\rho(r_c)g(r_c) \\ 0 & 0 & 0 \\ r_cY(r_c)+4\pi Gr_c\rho(r_c)\Phi(r_c)/g(r_c) & 0 & 4\pi Gr_c\rho(r_c) \end{bmatrix}.
\tag{37}
$$

We point out that while the second column in eq. (37) indicates that the tangential displacement at the bottom of the mantle is not restricted by the conditions in the core, the first and third columns are the two general solutions on the core side of the core–mantle boundary which are continuously transferred to the mantle side (Saito1974; Sun 1992).

Passing the solution from the core to the mantle, and propagating the result to the surface of the Earth, we finally have

$$
\begin{bmatrix} U(\xi_p) \\ aT(\xi_p) \end{bmatrix}\Big|_{r=a} = \exp(B_p\xi_p)\exp(B_{p-1}\xi_{p-1})\cdots\exp(B_1\xi_1)[B_c] \begin{bmatrix} c_1 \\ c_2 \\ c_3 \end{bmatrix}.
\tag{38}
$$

The three unknown coefficients c_i on the right-hand side of eq. (38) can be solved by the boundary conditions on the surface of the Earth $r = a$, which will be discussed later.

4.2 Layered and incompressible core

It can be shown that under the assumption of an incompressible core, the potential field in the core is independent of the elastic deformation and further satisfies the following first-order differential equations (Wu & Peltier 1982)

$$
\Phi' = \frac{4\pi G\rho}{g}\Phi - \frac{n+1}{r}\Phi + Q
$$
$$
Q' = \frac{8\pi G\rho(n-1)}{gr}\Phi + \frac{n-1}{r}Q - \frac{4\pi G\rho}{g}Q,
\tag{39}
$$

where again the density ρ can be any function of r, and the gravity g is related to the density via Newton's gravitational law (17).

This first-order differential system of equations is exactly the same as eq. (29). Therefore, it assumes the same initial solution when $r \leq r_0$, as in eq. (34) but for the function pairs (Φ, Q)

$$
\begin{bmatrix} \Phi \\ rQ \end{bmatrix} = \begin{bmatrix} r^n \\ 2(n-1)r^n \end{bmatrix}. \tag{40}
$$

Similarly, we subdivide the core into layers and assume that in each layer the density ρ is approximated as constant and the gravity is approximated as linear $g = kr$. Just like in the layered compressible core, this assumption is exact in case of a uniform core. We then arrive at the same matrix $[A]$ as in eq. (33). We therefore have the same propagating relation eq. (35) (one needs just to replace Y by Q in eq. 35). Once being propagated to the core–mantle boundary r_c, we obtain eq. (38), but with the new core–mantle boundary matrix $[B_c]$ being defined as

$$
[B_c] = \begin{bmatrix} -\Phi(r_c)/g(r_c) & 0 & 1 \\ 0 & 1 & 0 \\ \Phi(r_c) & 0 & 0 \\ 0 & 0 & r_c\rho(r_c)g(r_c) \\ 0 & 0 & 0 \\ r_cQ(r_c) & 0 & 4\pi Gr_c\rho(r_c) \end{bmatrix}. \tag{41}
$$

Thus, solutions for the incompressible and layered core case are derived.

We point out that, for a fixed mantle model, the layered compressible and layered incompressible cores predict exactly the same LLNs under the core–mantle conditions (37) and (41) presented in the paper. This is due to the fact that the first column in eq. (37) is a linear combination of the first and third columns of eq. (41).

4.3 Homogeneous and incompressible core

If we assume that the liquid core is homogeneous and incompressible, then the same solution (40) can be applied to the entire core. Making use of the continuity conditions on the core–mantle boundary $r = r_c$, we have, on the mantle side of $r = r_c$, the following relations

$$
U_L = -\frac{3r_c^{n-1}}{4\pi G\rho_c}c_1 + c_3; \quad U_M = c_2; \quad U_N = c_4
$$

$$
T_L = \frac{4\pi G\rho_c^2 r_c}{3}c_3; \quad T_M = 0; \quad T_N = 0
$$

$$
\Phi = r_c^n c_1; \quad Q = 2(n-1)r_c^{n-1}c_1 + 4\pi G\rho_c c_3 \tag{42}
$$

where again c_i $(i = 1-3)$ are the three coefficients to be determined by the boundary conditions applied on the surface of the Earth. Thus, in the propagating relation (38), the core-mantle boundary matrix $[B_c]$ for this simple homogeneous and incompressible core model is reduced to

$$
[B_c] = \begin{bmatrix} -\frac{3r_c^{n-1}}{4\pi G\rho_c} & 0 & 1 \\ 0 & 1 & 0 \\ r_c^n & 0 & 0 \\ 0 & 0 & \frac{4\pi G\rho_c^2 r_c^2}{3} \\ 0 & 0 & 0 \\ 2(n-1)r_c^n & 0 & 4\pi G\rho_c r_c \end{bmatrix}. \tag{43}
$$

5 LOAD LOVE NUMBERS

For the first two core models (layered compressible and layered incompressible), we can propagate the analytical solutions from the center of the core to the core–mantle boundary at $r = r_c$. Then for all the three core models (including the homogeneous incompressible core model), we can propagate the solution from the core–mantle boundary to the surface so that we finally have, on the surface of the Earth $r = a$ $(=r_p)$,

$$
\begin{bmatrix} U(\xi_p) \\ aT(\xi_p) \end{bmatrix} \Big|_{r=a} = \begin{bmatrix} A_1 \\ A_2 \end{bmatrix} \begin{bmatrix} c_1 \\ c_2 \\ c_3 \end{bmatrix}, \tag{44}
$$

where

$$
\begin{bmatrix} A_1 \\ A_2 \end{bmatrix} = \exp\left(B_p \xi_p\right) \exp\left(B_{p-1}\xi_{p-1}\right) \cdots \exp\left(B_1\xi_1\right) [B_c].
\tag{45}
$$

For the surface loading case, the boundary conditions for the expansion coefficients on the surface $r = a$ can be expressed as

$$
T_L(a) = -g_a C_n^m; \quad T_M(a) = 0
$$

$$
Q(a) = -4\pi G C_n^m,
\tag{46}
$$

where we have assumed that the product of the load height (e.g. tide height) and density (i.e. water density) as a single scalar function can be expanded as

$$
\gamma(\theta, \phi) = \sum_{n=0}^{\infty} \sum_{m=-n}^{n} C_n^m S(\theta, \phi),
\tag{47}
$$

where C_n^m are the expansion coefficients

Therefore, making use of the boundary conditions (46) at $r = a$, we can solve the three unknown coefficients c_i in eq. (44) by using the last three expressions. After that, the first three expressions in eq. (44) can be used to find U_L, U_M and Φ on the surface of the Earth at $r = a$.

By definition of the LLN (neglecting the prime sign in the LLN), we have the following expressions for the LLN (in proportion to the magnitude of the perturbed potential ψ_l)

$$
h_n = (2n + 1)U_L(a)g_a/(4\pi G C_n^m)
$$

$$
l_n = (2n + 1)U_M(a)g_a/(4\pi G C_n^m)
$$

$$
k_n = -[(2n + 1)\Phi(a)g_a/(4\pi G C_n^m) + 1].
\tag{48}
$$

We point out that eq. (48) is the expression for the LLNs of degrees $n > 1$. For $n = 1$, since the rigid-body motion is involved, one can solve the three first-degree LLNs by assuming that the center of mass of the Earth plus the surface load (CE) is fixed in space as in Farrell (1972) or by simply using the centre of mass (CM) system as in Spada *et al.* (2011). Detailed discussions on the perturbed potential and definition of the LLNs for $n = 1$ are given in Appendix C. The analytical solution and the LLN for degree $n = 0$ are also discussed and are presented in Appendix D.

6 NUMERICAL RESULTS

6.1 LLNs of the benchmark example

The analytical solutions are coded in MATLAB and are first checked against the benchmark numerical results in Spada *et al.* (2011). The simple earth model contains four incompressible layers in the mantle over a homogeneous and incompressible core. Each mantle layer is isotropic with a constant density and a shear modulus. This benchmark model is taken from table 3 of Spada *et al.* (2011) with its details being also provided in Appendix E for easy reference. We point out that, different from Spada *et al.* (2011), here we assumed that, in each layer, the density follows the $1/r$-variation as in eq. (15) with $\bar{\rho}$ being the constant density in Spada *et al.* (2011). The gravity in each layer is constant, being the average over the layer governed by the Newton's law (17). We remark that while piecewise constant density distribution in Spada *et al.* (2011) may not be the best approximation to the real earth model, this five-layer model provides an excellent benchmark and it is a good reference for assessing the accuracy of a code in predicting the deformation of the Earth subject to mass and tidal loading.

In order to apply our analytical solutions and the corresponding code to this piecewise constant layering structures, we approximate each layer of constant density by different numbers of layers where their density is proportional to $1/r$ and the gravity is constant. Again, the average constant gravity in each layer is calculated via Newton's gravitational law (17) up to that layer. In order to prove that the present approach works, we want first to measure the effect of the approximation for the density and of the decoupling of density and gravity on the LLN. This is performed using the same number of layers as the original benchmark model.

The second step is to show that these effects can be made arbitrarily small by increasing the number of artificial layers. This shows that the benchmark model can be effectively approximated arbitrarily well by a model with the same elastic properties, but an artificially fine layering in the density, necessary to be able to apply the analytic solutions layer by layer. To do so, we use the following simple j-step subdivision process: at the step j, we subdivide each of the 4 mantle layers into 2^j equally spaced sublayers. Each of this sub-layer has the same elastic properties as the original one. But for each of them, a finer approximation of the density profile according to eqs (15) and (16) is obtained. In this way, at step j, the mantle consists of 4×2^j layers, with step $j = 0$ being the original five-layer benchmark model.

The calculated LLNs ($-h_n$, $-l_n$, and $-k_n$) from our code are listed in Tables 1 and 2. While Table 1 shows the LLNs for degrees $n = 2$ and 3 at different subdivision steps j, Table 2 lists, at step $j = 18$, the LLNs calculated by our code as compared to those from Spada *et al.* (2011). It is observed from Table 1 that, with increasing step j or increasing layer numbers, our LLNs are clearly convergent to the benchmark results. Furthermore, they are all convergent monotonically, in terms of magnitude, from above to (except for $j < 4$) the benchmark LLNs

Table 1. LLNs for degrees 2 and 3 of the five-layer earth model used in Spada *et al.* (2011) obtained by the present analytical solutions with different refinements. More specifically, the constant density in each layer is approximated by a density variation of $1/r$ with different subdivisions of layers following 4×2^j in each subdividing step j. The final row (labelled as SP) contains the values from Spada *et al.* (2011).

j	$-h_2(\times 10^{-1})$	$-l_2(\times 10^{-1})$	$-k_2(\times 10^{-1})$	$-h_3(\times 10^{-1})$	$-l_3(\times 10^{-2})$	$-k_3(\times 10^{-1})$
0	4.54412295	1.32299524	2.40720605	4.64747818	6.96395022	1.61080459
1	4.54655807	1.29472337	2.43426482	4.62071528	6.79989917	1.63225980
2	4.54447274	1.28625243	2.43977390	4.61244771	6.74702937	1.63718893
3	4.54222021	1.28366344	2.44047219	4.60900655	6.73150117	1.63809774
4	4.54078890	1.28279562	2.44031804	4.60744423	6.72665777	1.63816950
5	4.53999750	1.28246932	2.44011625	4.60670253	6.72497713	1.63811055
6	4.53958293	1.28233312	2.43998426	4.60634155	6.72432270	1.63805743
7	4.53937093	1.28227177	2.43991050	4.60616353	6.72404200	1.63802496
8	4.53926375	1.28224277	2.43987168	4.60607513	6.72391327	1.63800725
9	4.53920987	1.28222870	2.43985179	4.60603109	6.72385182	1.63799803
10	4.53918285	1.28222177	2.43984172	4.60600911	6.72382182	1.63799333
11	4.53916933	1.28221833	2.43983665	4.60599813	6.72380700	1.63799095
12	4.53916256	1.28221661	2.43983411	4.60599264	6.72379963	1.63798976
13	4.53915917	1.28221576	2.43983284	4.60598990	6.72379596	1.63798916
14	4.53915748	1.28221533	2.43983220	4.60598852	6.72379413	1.63798886
15	4.53915663	1.28221512	2.43983189	4.60598784	6.72379321	1.63798871
16	4.53915621	1.28221501	2.43983173	4.60598749	6.72379276	1.63798864
17	4.53915600	1.28221496	2.43983165	4.60598733	6.72379253	1.63798860
18	4.53915588	1.28221493	2.43983160	4.60598723	6.72379240	1.63798858
SP	4.5391558	1.2822149	2.4398316	4.6059872	6.7237923	1.6379886

Table 2. Comparison of LLNs obtained at refinement step $j = 18$ and those in parentheses reported in Spada *et al.* (2011). Note that the LLN l of degree $n = 256$ was convergent at an early step $j = 16$ with its value being $-2.06125011 \times 10^{-4}$. The results for degree $n = 1$ are based on the centre of mass (CM) reference system.

n	$-h_n$	$-l_n$	$-k_n$
1	1.01748425 (1.0174843)	1.08122247 (1.0812225)	1.0 (1.0)
2	4.53915588E-1 (4.5391558E-1)	1.28221493E-1 (1.2822149E-1)	2.43983160E-1 (2.4398316E-1)
3	4.60598723E-1 (4.6059872E-1)	6.72379240E-2 (6.7237923E-2)	1.63798858E-1 (1.6379886E-1)
4	4.53094444E-1 (4.5309444E-1)	5.54990941E-2 (5.5499093E-2)	1.17385746E-1 (1.1738574E-1)
5	4.69288024E-1 (4.6928802E-1)	5.21188443E-2 (5.2118844E-2)	9.47296337E-2 (9.4729633E-2)
6	5.02508648E-1 (5.0250864E-1)	4.94002474E-2 (4.9400247E-2)	8.27989974E-2 (8.2798997E-2)
15	0.92394970 (0.92394969)	2.53387344E-2 (2.5338734E-2)	5.61682425E-2 (5.6168242E-2)
30	1.38473104 (1.3847310)	8.09246886E-3 (8.0924688E-3)	4.09208519E-2 (4.0920852E-2)
64	1.66800129 (1.6680013)	3.03560966E-3 (3.0356095E-3)	2.24640902E-2 (2.2464090E-2)
128	1.92106041 (1.9210604)	1.39764804E-3 (1.3976479E-3)	1.25577911E-2 (1.2557791E-2)
256	2.19042635 (2.1904264)	2.06124159E-4 (2.0612502E-4)	7.06846187E-3 (7.0684622E-3)

listed in Spada *et al.* (2011). It is further noticed from Table 1 that using the benchmark five-layer model ($j = 0$) directly can already provide very good results as compared to those in Spada *et al.* (2011), with a relative error less than 4 per cent. If we consider all LLN values for n from 1 to 256, the largest absolute difference between our code at step $j = 18$ and those by Spada *et al.* (2011) is less than 10^{-8} (Table 2). This partially validates that the analytical solutions presented in this paper are accurate since the difference between our solution and the benchmark is only related to the model approximation on the density and gravity variations.

With this test we showed that the solution built in the previous sections can be successfully applied to the layered incompressible model. The two approximations that are necessary to obtain the analytic solution for a homogeneous Earth with a density profile of the Darwin's law form (eq. 15) and to extend the solution to the layered Earth (decoupling g and ρ) would at most introduce a relative error less than 4 per cent. Most importantly, we showed that this error can be made arbitrarily small by increasing the density layering and that the solution converges to the exact one, in contrast to what happens with the Gilbert & Backus solution (Gilbert & Backus 1968; Cambiotti *et al.* 2009). Since the
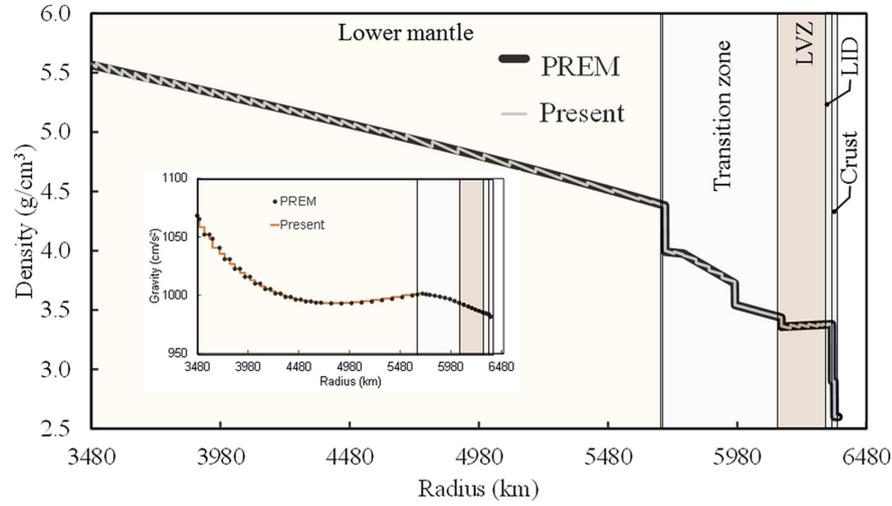
Figure 3. Density distribution in the Earth mantle based on 56 layers featuring $1/r$ variation in density in each layer versus the PREM model. Inserted is the corresponding piecewise constant gravity distribution averaged over the calculated gravity in each layer via the Newton's gravitational law versus that of the PREM model.

solution is based on the analytic expressions, it can be implemented so that the additional computational cost of this artificial layering is small. Furthermore, the computation takes the same number of steps (and therefore the same time), independent of the harmonic degree.

The comparison with the benchmark model was therefore crucial to check the approach, and the implementation. Anyway the benchmark provides a check only for the incompressible models, for which (at least for isotropic material) an analytic solution already exists. In the next subsection, we will calculate the LLNs for a set of earth models, combining different cores, incompressible, compressible, with isotropic and transverse isotropic mantles. For some of these models it is also possible to compare the results with those obtained via a numerical code.

6.2 LLNs of various earth models

We now apply the solutions obtained in the previous sections to calculate the LLNs corresponding to the PREM earth model (Dziewonski & Anderson 1981). In the mantle, we use 56 layers to approximate its density distribution in the PREM model as listed in table I of Dziewonski & Anderson (1981), that is the polynomial representation, with the uniform elastic properties being just those in the corresponding layer and the constant gravity being the average of the layer. We further point out that these parameters are valid at a reference period of 1 s and that for depths from 24.4 to 220 km, the material property is transversely isotropic with their properties being listed in Dziewonski & Anderson (1981). The elastic constants of eq. (4) are related to those (A, C, L, N, and F) defined in Dziewonski & Anderson (1981) as

$$A = c_{11}; \quad C = c_{33}; \quad L = c_{44}; \quad N = c_{66}; \quad F = c_{13}. \tag{49}$$

The top water layer is replaced by an elastic layer with properties similar to the layer below (i.e. Wang *et al.* 2012). We point out that while elastic constants A and C are related to the velocities of P waves propagating perpendicular and parallel to the axis of symmetry (i.e. the radial direction), N and L are related to the shear-wave velocities. Elastic constant F is a function of the velocities at intermediate incidence angles (Dziewonski & Anderson 1981). Fig. 3 shows the density distribution in the entire mantle based on our $1/r$ variation using 56 mantle layers vs the PREM model in terms of polynomial representation. The corresponding comparison on the gravity is also shown in this figure. We point out that the difference between our 56 layered mantle model and the PREM model for both the density and gravity is at most 0.6 per cent.

For the core of the Earth, we use 26 layers to approximate its gravity variation. For this case, the gravity in each layer is approximated as $g(r) = kr$ variation with constant density. Fig. 4 shows the gravity distribution in the core based on our kr-variation using 26 layers vs the PREM model. The corresponding density is also shown in this figure. The maximum difference between our 26 layer core model and the PREM model for both the density and gravity is again less than 1 per cent.

Based on the mantle and core models along with the core–mantle boundary conditions, we have calculated the LLNs for the following five earth models. They are

Model 1 is symbolically indicated by **56CT-26C:** 56 mantle layers which are **C**ompressible and **T**ransversely isotropic, over 26 core layers which are **C**ompressible. The transversely isotropic properties exist from 24.4 to 220 km in the mantle with properties being taken from table IV in PREM model, evaluated at a reference periods of 1 s (Dziewonski & Anderson 1981);

Model 2 is symbolically indicated by **56C-26C:** 56 mantle layers which are **C**ompressible and isotropic, over 26 core layers which are **C**ompressible;

Model 3 is symbolically indicated by **56C-UInc:** 56 mantle layers which are **C**ompressible and isotropic, over a **U**niform **Inc**ompressible core;
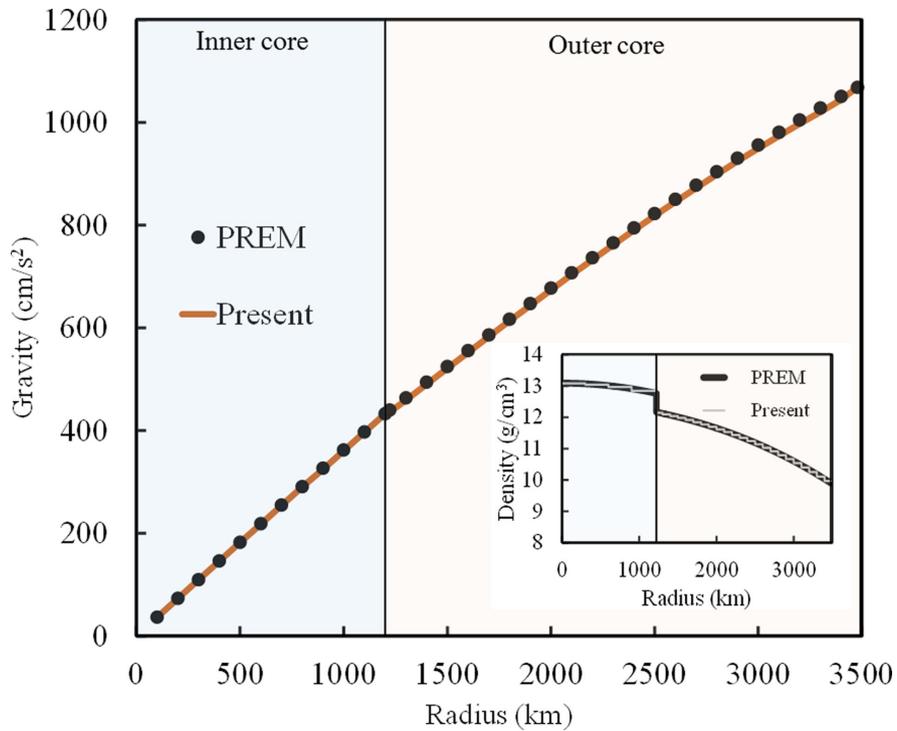
Figure 4. Gravity distribution in the core using 26-layers featuring linear variation in *r* versus the PREM model. Inserted is the corresponding piecewise constant density distribution versus that of the PREM model.
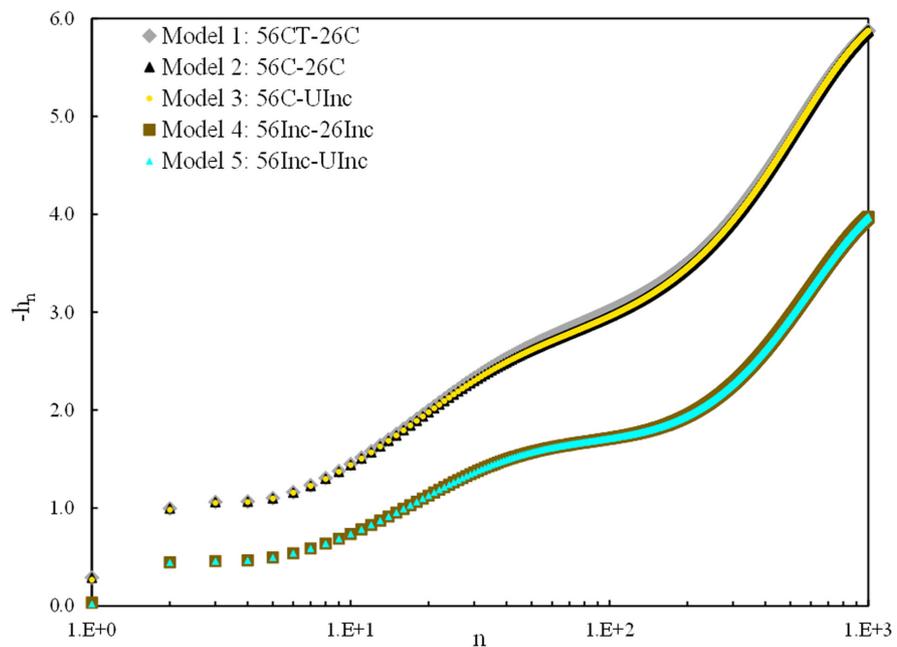

Figure 5. Variation of LLNs $-h_n$ for different earth models (from degrees $n = 1$ to 1000).

Model 4 is symbolically indicated by **56Inc-26Inc:** 56 mantle layers which are **Inc**ompressible and isotropic, over 26 core layers with are **Inc**ompressible;

Model 5 is symbolically indicated by **56Inc-UInc:** 56 mantle layers which are **Inc**ompressible and isotropic, over a **U**niform **Inc**ompressible core.

For easy future reference, we have listed the model parameters for Models 56CT, 56C, and 26C in Appendix F and have further presented the solutions for the case of large degree *n* in Appendix G. The complete list of LLNs for all the five models can be obtained from the first author at pan2@uakron.edu.

Figs 5–7 show the variation of the LLNs ($-h_n$, nl_n, and $-nk_n$) from $n = 1$ to 1000 for the five different earth models with some of the selected values from $n = 1$ to 6000 being listed in Tables 3–5 for further reference (including h_0). The results for degree $n = 1$ are based
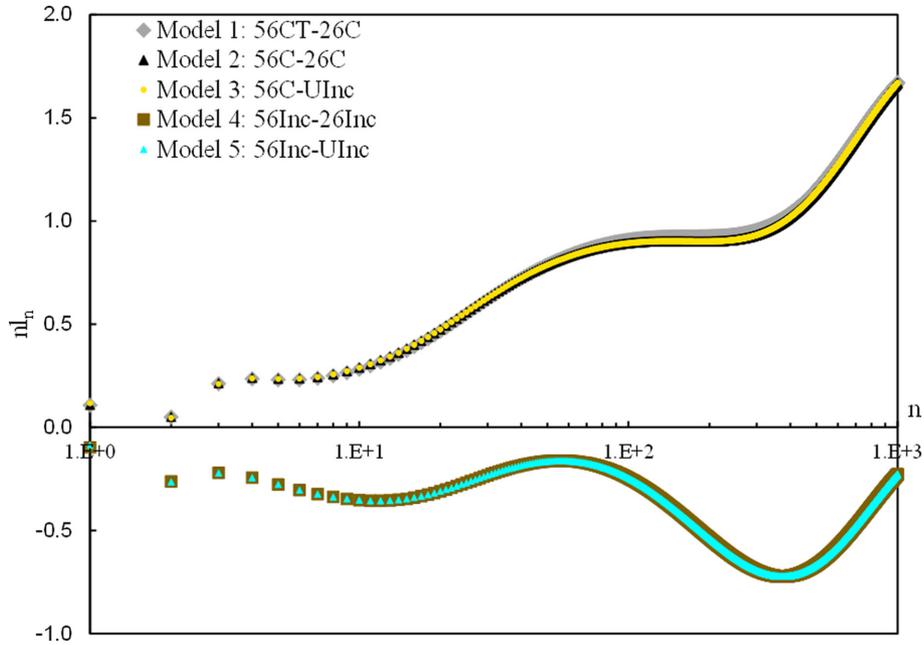
Figure 6. Variation of LLNs nl_n for different earth models (from degrees $n = 1$ to 1000).
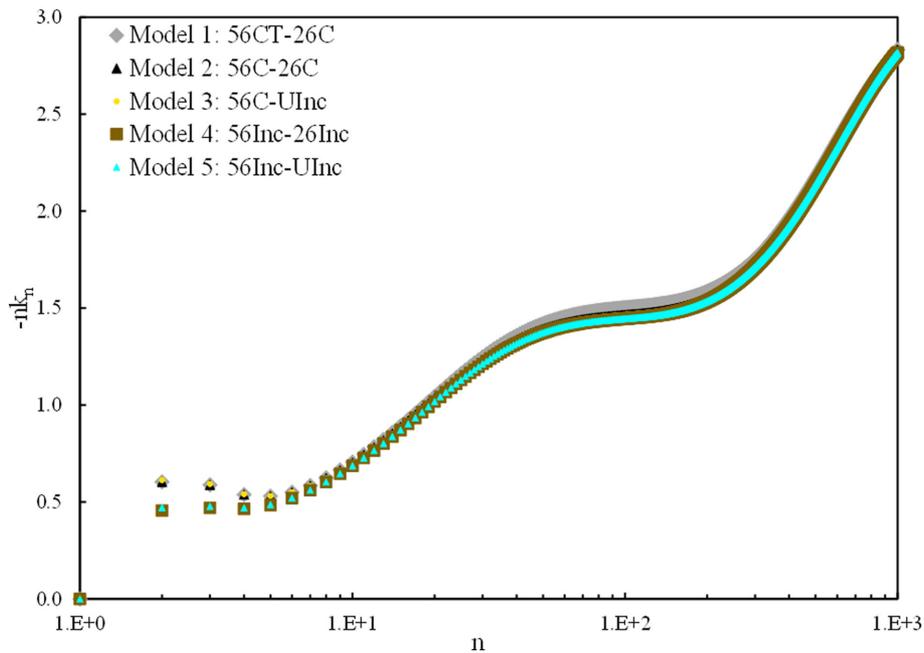

Figure 7. Variation of LLNs $-nk_n$ for different earth models (from degrees $n = 1$ to 1000).

on the center of Earth (CE) system (see Appendix C). We further point out that for the transversely isotropic Earth Model 1 (56CT-26C), our code can run only to n slightly larger than 2000. However, by running our code for Models 1 and 2, we noticed that, the LLNs are convergent to each other with increasing n. In other words, the LLNs of the transversely isotropic earth model are nearly the same as those of the corresponding isotropic Earth Model 2 (56C-26C) for $n > 2000$. Furthermore, for Models 3 (56C-UInc) and 5 (56Inc-UInc), we have also listed in parentheses the LLNs from the program E-CL0V3RS v3.5 by Barletta and Bordoni, that has been benchmarked, using the Earth mantle modes with 56 layers. In using the E-CL0V3RS program, the density in each mantle layer is constant and the gravity is calculated in each layer exactly via Newton's gravitational law (17). By comparing our LLNs to those from E-CL0V3RS in Tables 3–5, we observe that the first two to three digits are exactly the same. This gives a measure of the effect of the assumptions necessary to find the analytic solution for a 56 layer model. This partially verifies that, since our model parameters (density and gravity) deviate by less than 1 per cent as compared to the PREM model, the listed LLNs should have a relative error less than 1 per cent.

Table 3. Load Love numbers $-h_n$ of different earth models. LLNs in parentheses are calculated from program E-CL0V3RS v3.5 by Barletta and Bordoni.

n	Model 1: 56CT-26C	Model 2: 56C-26C	Model 3: 56C-UInc	Model 4: 56Inc-26Inc	Model 5: 56Inc-UInc
0	0.13431	0.13396	0.10811	0.00000	0.00000
1	0.28897	0.28792	0.26673 (0.26613)	0.03298	0.01931 (0.01899)
2	0.99588	0.99522	0.98290 (0.98082)	0.44467	0.44323 (0.44233)
3	1.06143	1.06009	1.05313 (1.05136)	0.45863	0.45722 (0.45651)
4	1.06707	1.06459	1.06200 (1.06043)	0.46523	0.46472 (0.46408)
5	1.10223	1.09857	1.09765 (1.09613)	0.49466	0.49449 (0.49383)
6	1.16177	1.15699	1.15666 (1.15511)	0.53787	0.53781 (0.53710)
8	1.30555	1.29864	1.29860 (1.29690)	0.63679	0.63678 (0.63596)
10	1.44826	1.43923	1.43923 (1.43736)	0.73499	0.73499 (0.73405)
18	1.90898	1.89131	1.89131 (1.88888)	1.06312	1.06312 (1.06177)
32	2.37691	2.34508	2.34508 (2.34208)	1.39577	1.39577 (1.39400)
56	2.72208	2.67414	2.67414 (2.67074)	1.60050	1.60050 (1.59848)
100	3.01388	2.95804	2.95804 (2.95429)	1.71105	1.71105 (1.70889)
180	3.40834	3.35723	3.35723 (3.35299)	1.88664	1.88664 (1.88426)
325	4.08824	4.05323	4.05323 (4.04810)	2.35553	2.35553 (2.35256)
550	4.96895	4.95400	4.95400 (4.94774)	3.10235	3.10235 (3.09844)
1000	5.87847	5.87699	5.87699 (5.86956)	3.97244	3.97244 (3.96742)
2000	6.19356	6.19355	6.19355 (6.18572)	4.30131	4.30131 (4.29587)
3000	–	6.20356	6.20356 (6.19571)	4.31325	4.31325 (4.30779)
4000	–	6.20439	6.20439 (6.19654)	4.31477	4.31477 (4.30932)
5000	–	6.20478	6.20478 (6.19694)	4.31559	4.31559 (4.31013)
6000	–	6.20504	6.20504 (6.19719)	4.31613	4.31613 (4.31067)

Furthermore, the following interesting features can be observed from these tables and figures:

(1) As expected, for a fixed core model, mantle compressibility substantially affects the LLNs (e.g. Tanaka *et al.* 2011). The property that has the strongest effect is compressibility: the results fell into two distinct families, one for the compressible and one for the incompressible mantle. This can be observed by comparing Models 1–3 (56CT-26C, 56C-26C, 56C-UInc) to Models 4–5 (56Inc-26Inc, 56Inc-UInc). More specifically, an incompressible mantle remarkably reduces the magnitude of LLNs h_n (Fig. 5) and even changes the sign of LLNs l_n (Fig. 6). As such, assumption of an incompressible mantle needs to be carefully justified. However, the effect of mantle compressibility on the perturbed gravity potential is nearly negligible (Fig. 7).

(2) For a given mantle model, the effect of the details of different core modelling (layering, compressibility) is very small. The very simple uniform incompressible core model yields very similar results as a layered incompressible and layered compressible core models do. The only obvious difference is for the lower degree LLNs from 1 to 4 (including h_0), giving therefore effect only at extremely long wavelength, at the global level. This substantial independence on the modelling details proves that it is not necessary to invoke very complex core model in most applications. This further indicates that it is possible to calculate the correct LLNs without much computational efforts. In other words, for LLNs with lower degrees ($n = 1$ to 4, including h_0), we use the detailed layered core model; but for large degrees n, we can simply use the equivalent homogeneous incompressible core model.

(3) For the given core model, mantle anisotropy (Model 56CT-26C) affects all the three types of LLNs. More specifically, the PREM anisotropy increases the amplitude of the LLNs as compared to the corresponding isotropic case (except for a few low-degree LLNs nl_n). Furthermore, its influence on nk_n and h_n is larger than for nl_n. The difference is small for very low n, and peaks around degree $n = 100$, but remains noticeable up to degree $n \sim 1000$. After that the LLNs converge to the isotropic ones. This reflects the physics of the problem, since the anisotropic layers are present in the model only for the depths between 220 and 24.4 km, which corresponds roughly to an interval of harmonic degree n between 90 and 800. Moreover, we notice that the relative effect (difference in percentage) is different in the three components of the LLN solution, and this could be very useful in various particular problems to better explain the observables, with respect to the isotropic case.

7 CONCLUSIONS

In this paper, we have presented an analytical solution for the deformation of a transversely isotropic, layered and self-gravitating Earth under concentrated surface loading. The solution covers both incompressible and compressible mantle and core, and reduces to the solution for the traditional isotropic mantle when eq. (5) is satisfied. The solution is derived in terms of the vector spherical harmonics with the expansion coefficients being obtained via the propagator matrix method. We derived the propagator matrices under the assumptions that in each mantle layer the density varies as $1/r$ and the gravity is constant, and that in each core layer the gravity is linearly proportional to r with a constant

Table 4. Load Love numbers nl_n of different earth models. LLNs in parentheses are calculated from program E-CL0V3RS v3.5 by Barletta and Bordoni. For all five models, $l_0 = 0$.

n	Model 1: 56CT-26C	Model 2: 56C-26C	Model 3: 56C-UInc	Model 4: 56Inc-26Inc	Model 5: 56Inc-UInc
1	0.10710	0.10789	0.11652 (0.11652)	−0.09740	−0.08677 (−0.08647)
2	0.04940	0.05096	0.04608 (0.04590)	−0.26289	−0.26449 (−0.26408)
3	0.21121	0.21407	0.20974 (0.20926)	−0.22076	−0.22188 (−0.22160)
4	0.23529	0.23903	0.23697 (0.23653)	−0.24400	−0.24453 (−0.24421)
5	0.23060	0.23503	0.23421 (0.23383)	−0.27731	−0.27752 (−0.27714)
6	0.23069	0.23575	0.23543 (0.23508)	−0.30421	−0.30428 (−0.30387)
8	0.25036	0.25657	0.25653 (0.25618)	−0.33752	−0.33753 (−0.33708)
10	0.28131	0.28848	0.28847 (0.28809)	−0.35277	−0.35278 (−0.35231)
18	0.42879	0.43756	0.43756 (0.43698)	−0.32649	−0.32649 (−0.32607)
32	0.64379	0.64993	0.64993 (0.64908)	−0.22035	−0.22035 (−0.22008)
56	0.81595	0.81281	0.81281 (0.81175)	−0.16198	−0.16198 (−0.16178)
100	0.90690	0.89270	0.89270 (0.89156)	−0.24611	−0.24611 (−0.24580)
180	0.92269	0.90118	0.90118 (0.90003)	−0.48846	−0.48846 (−0.48785)
325	0.97016	0.94958	0.94958 (0.94837)	−0.71101	−0.71101 (−0.71011)
550	1.21738	1.20682	1.20682 (1.20529)	−0.62448	−0.62448 (−0.62369)
1000	1.67013	1.66893	1.66893 (1.66682)	−0.22774	−0.22774 (−0.22745)
2000	1.88030	1.88031	1.88031 (1.87793)	−0.01086	−0.01086 (−0.01085)
3000	–	1.88737	1.88737 (1.88498)	−0.00231	−0.00231 (−0.00231)
4000	–	1.88752	1.88752 (1.88513)	−0.00162	−0.00162 (−0.00162)
5000	–	1.88753	1.88753 (1.88514)	−0.00129	−0.00129 (−0.00129)
6000	–	1.88752	1.88752 (1.88513)	−0.00108	−0.00108 (−0.00108)

Table 5. Load Love numbers $-nk_n$ of different earth models. LLNs in parentheses are calculated from program E-CL0V3RS v3.5 by Barletta and Bordoni. For all five models, $k_0 = 0$.

n	Model 1: 56CT-26C	Model 2: 56C-26C	Model 3: 56C-UInc	Model 4: 56Inc-26Inc	Model 5: 56Inc-UInc
1	0.00000	0.00000	0.00000 (0.00000)	0.00000	0.00000 (0.00000)
2	0.60363	0.60429	0.61288 (0.61178)	0.45550	0.47096 (0.47028)
3	0.58788	0.58829	0.59277 (0.59208)	0.46900	0.47748 (0.47703)
4	0.53814	0.53805	0.54075 (0.54029)	0.46452	0.46887 (0.46853)
5	0.52981	0.52923	0.53049 (0.53011)	0.48451	0.48640 (0.48610)
6	0.55041	0.54937	0.54987 (0.54952)	0.51961	0.52035 (0.52005)
8	0.62413	0.62216	0.62223 (0.62187)	0.60337	0.60347 (0.60314)
10	0.70583	0.70286	0.70287 (0.70247)	0.68671	0.68672 (0.68635)
18	0.98821	0.98042	0.98042 (0.97987)	0.96279	0.96279 (0.96226)
32	1.27581	1.25853	1.25853 (1.25785)	1.23858	1.23858 (1.23792)
56	1.44304	1.41341	1.41341 (1.41267)	1.39449	1.39449 (1.39376)
100	1.50153	1.46460	1.46460 (1.46385)	1.44509	1.44509 (1.44436)
180	1.56024	1.52598	1.52598 (1.52522)	1.50791	1.50791 (1.50715)
325	1.80330	1.78011	1.78011 (1.77926)	1.76420	1.76420 (1.76335)
550	2.26792	2.25806	2.25806 (2.25710)	2.23564	2.23564 (2.23469)
1000	2.83225	2.83126	2.83126 (2.83032)	2.81647	2.81647 (2.81554)
2000	3.04399	3.04399	3.04399 (3.04307)	3.04219	3.04219 (3.04127)
3000	–	3.05191	3.05191 (3.05075)	3.05099	3.05099 (3.04984)
4000	–	3.05309	3.05309 (3.05173)	3.05241	3.05241 (3.05105)
5000	–	3.05375	3.05375 (3.05224)	3.05321	3.05321 (3.05170)
6000	–	3.05418	3.05418 (3.05258)	3.05372	3.05372 (3.05213)

density. Under these assumptions it is possible to combine the analytic solutions for each layer into a solution for the layered Earth. This 'Darwin law' assumption for the density profile in the mantle, and especially the necessary decoupling of the density and gravity inside each layer, has an effect on the global solution, which we measured by comparing the results obtained based on our MATLAB implementation with the LLNs from Spada *et al.* (2011). As we showed, the effect of the approximation is small but not negligible (about 4 per cent) for the benchmark incompressible model, which is anyway a worst case scenario for the comparison, as it consists only 5 thick uniform layers. However, with a finer density-layering structure we obtain a solution that converges to the exact result. This method allows us to compute

efficiently the LLNs for models where both the mantle and core can be uniform or layered, compressible and incompressible, with isotropic or transversely isotropic mantle structure. Transverse isotropy is a special form of material anisotropy that is present in the mantle according to the PREM specifications.

We applied the method to a set of previously-adopted earth models. Here we used a simple PREM-based layering that gives an estimated discrepancy with respect to the correct PREM results, much below 1 per cent as shown in the paper. Furthermore, whenever possible, we compared our results with those obtained via a benchmarked numerical software (E-CL0V3RS). Our calculation and comparison of the LLNs showed the following interesting features for the PREM earth models:

(1) The surface LLNs are almost insensitive to the details of the core model, apart from the very low degrees. This means that for a given mantle structure, a uniform incompressible core model yields very similar results as a layered incompressible core or a layered compressible core model does when the degree is larger than 4. Therefore both refined layering and compressibility in the core play a minor role and may only be useful in a very global spatial scale. This result is expected because the sensitivity of the solution to a specific layer at given wavelength depends on the depth of the layer, and most local and regional phenomena are insensitive to the lower mantle structure.

(2) The property that has the largest effect on the LLN is, as expected (Tanaka *et al.* 2011), the compressibility in the mantle. All the models fall into two clear families. An incompressible mantle remarkably reduces the magnitude and even changes the sign of many LLNs.

(3) We also investigate the effect of mantle material transverse isotropy on the LLNs. For the given core model, this specific mantle anisotropy affects all the three types of LLNs with a small but measurable effect for all degrees to $n \sim 1000$. For the PREM model, the difference of the LLNs between anisotropic and isotropic cases is not uniform, but peaks around degree $n = 100$. More specifically, the PREM anisotropy increases the amplitude of the LLNs as compared to the corresponding isotropic case (expect for a few low-degree nl_n) and its influence on nk_n and h_n seems larger than for nl_n. This suggests that mantle material anisotropy could give a significant contribution, especially in local applications, when deviation from the average isotropic PREM model is significant, especially in the shallower layer.

REFERENCES

Anderson, D.L., 1961. Elastic wave propagation in layered anisotropic media, *J. geophys. Res.,* **66,** 2953–2963.

Cambiotti, G., Barletta, V.R., Bordoni, A. & Sabadini, R., 2009. A comparative analysis of the solutions for a Maxwell Earth: the role of the advection and buoyancy force, *Geophys. J. Int.,* **176,** 995–1006.

Chen, J.Y., Pan, E. & Heyliger, P.R., 2015. Static deformation of a spherically anisotropic and multilayered magneto-electro-elastic hollow sphere, *Int. J. Solids Struct.,* **60–61,** 66–74.

Dziewonski, A.M. & Anderson, D.L., 1981. Preliminary reference Earth model, *Phys. Earth planet. Inter.,* **25,** 297–356.

Farrell, W.E., 1972. Deformation of the Earth by surface loads, *Rev. Geophys. Space Phys.* **10,** 761–797.

Gantmacher, F.R., 1977. *The Theory of Matrices*, Vol. 1. 374 pp., AMS Chelsea Publishing.

Gilbert, F. & Backus, G., 1968. Elastic-gravitational vibrations of a radially stratified sphere, in *Dynamics of Stratified Solids*. pp. 82–95, ed. Herrmann, G., American Society of Mechanical Engineers.

Guo, J.Y., Li, Y.B., Huang, Y., Deng, H.T., Xu, S.Q & Ning, J.S., 2004. Green's function of the deformation of the Earth as a result of atmospheric loading, *Geophys. J. Int.,* **159,** 53–68.

Longman, I.M., 1963. A Green's function for determining the deformation of the earth under surface mass loads. 2. Computations and numerical results, *J. geophys. Res.,* **68,** 485–496.

Martinec, Z., 2000. Spectral–finite element approach for three-dimensional viscoelastic relaxation in a spherical Earth, *Geophys. J. Int.,* **142,** 117–141.

Martinec, Z., Thoma, M. & Wolf, D., 2001. Material versus local incompressibility and its influence on glacial-isostatic adjustment, *Geophys. J. Int.,* **144,** 136–156.

Nield, G.A. *et al.*, 2014. Rapid bedrock uplift in the Antarctic Peninsula explained by viscoelastic response to recent ice unloading, *Earth planet. Sci. Lett.,* **397,** 32–41.

Pan, E., 1989. Static response of a transversely isotropic and layered half-space to general surface loads, *Phys. Earth planet. Inter.,* **54,** 353–363.

Pan, E. & Chen, W.Q., 2015. *Static Green's Functions in Anisotropic Media,* 337 pp., Cambridge Univ. Press.

Pan, E., Ding, Z. & Wang, R., 1986. The response of a spherically stratified earth model to potential body forces and surface loads, *Acta Scientiarum Naturalium, Universitis Pekinensis,* **22,** 66–79 (in Chinese with English abstract).

Riva, R.E.M. & Vermeersen, L.L.A., 2002. Approximation method for high-degree harmonics in normal mode modeling, *Geophys. J. Int.,* **151,** 309–313.

Saito, M., 1974. Some problems of static deformation of the Earth, *J. Phys. Earth,* **22,** 123–140.

Spada, G. *et al.*, 2011. A benchmark study for glacial isostatic adjustment codes, *Geophys. J. Int.* **185,** 106–132.

Sun, W., 1992. Potential and gravity changes caused by dislocations in spherically symmetric earth models, *Bull. Earthq. Res. Inst. Univ. Tokyo,* **67,** 89–238.

Takeuchi, H. & Saito, M., 1972. Seismic surface waves, in *Methods in Computational Physics*, Vol. 11, pp. 217–295, ed. Bolt, B.A., Academic Press.

Tanaka, Y., Klemann, V., Martinec, Z. & Riva, R.E.M., 2011. Spectral-finite element approach to viscoelastic relaxation in a spherical compressible Earth: application to GIA modeling, *Geophys. J. Int.,* **184,** 220–234.

Ulitko, A. F., 1979. *Method of Special Vector Functions in Three-Dimensional Elasticity,* 264 pp. Naukova Dumka (in Russian).

Vermeersen, L.L.A. & Mitrovica, J.X., 2000. Gravitational stability of spherical self-gravitating relaxation models, *Geophys. J. Int.,* **142,** 351–360.

Wang, H.S., Xiang, L.W., Jia, L.L., Jiang, L.M., Wang, Z.Y., Hu, B. & Gao, P., 2012. Load Love numbers and Green's functions for elastic Earth models PREM, isap91, ak135, and modified models with refined crustal structure from Crust 2.0. *Comput. Geosci.*, **49**, 190–199.

Watson, H.R. & Singh, S.J., 1972. Static deformation of a multilayered sphere by internal sources, *Geophys. J. R. astr. Soc.*, **27**, 1–14.

Wu, P. & Peltier, W.R., 1982. Viscous gravitational relaxation, *Geophys. J. R. astr. Soc.*, **70**, 435–485.

APPENDIX A: SPHERICAL HARMONIC FUNCTION AND THE CORRESPONDING VSH

We present the spherical harmonic function and the corresponding VSH in this appendix as reference. The spherical harmonic function and the associated Legendre function are well-known but people are using them with different definitions and different normalization factors. In this paper and in the VSH eq. (7), the normalized spherical harmonic function S is defined by

$$S(\theta, \phi; n, m) = \sqrt{\frac{(2n+1)(n-m)!}{4\pi(n+m)!}} P_n^m(\cos\theta)e^{im\phi} \qquad |m| \leq n; \quad n = 0, 1, 2, \ldots \tag{A1}$$

The associated Legendre function P_n^m in eq. (A1) is defined as

$$P_n^m(x) = (-1)^m(1-x^2)^{m/2}\frac{d^m}{dx^m}P_n(x); (m \geq 0), \tag{A2}$$

where P_n is the Legendre function of nth degree. Eq. (A2) holds for any positive m; when this index is negative, the associated function is defined in terms of its positive one as

$$P_n^{-m}(\cos\theta) = (-1)^m\frac{(n-m)!}{(n+m)!}P_n^m(\cos\theta); (m \geq 0). \tag{A3}$$

In so doing, one can define

$$S(\theta, \phi; n, -m) = (-1)^m \bar{S}(\theta, \phi; n, m), \tag{A4}$$

where an overbar denotes complex conjugate, giving as

$$\bar{S}(\theta, \phi; n, m) = \sqrt{\frac{(2n+1)(n-m)!}{4\pi(n+m)!}} P_n^m(\cos\theta)e^{-im\phi} \qquad |m| \leq n; \quad n = 0, 1, 2, \ldots. \tag{A5}$$

It is noted that the scalar function S satisfies the following Helmholtz equation

$$\frac{\partial^2 S}{\partial\theta^2} + \cot\theta\frac{\partial S}{\partial\theta} + \frac{1}{\sin^2\theta}\frac{\partial^2 S}{\partial\phi^2} + n(n+1)S = 0. \tag{A6}$$

It is easy to show that the VSH (7) are complete and orthogonal in the following sense.

$$\int_0^{2\pi} d\phi \int_0^{\pi} \boldsymbol{L}(\theta, \phi; n, m) \cdot \bar{\boldsymbol{L}}(\theta, \phi; n', m') \sin\theta d\theta = \delta_{nn'}\delta_{mm'}$$

$$\int_0^{2\pi} d\phi \int_0^{\pi} \boldsymbol{M}(\theta, \phi; n, m) \cdot \bar{\boldsymbol{M}}(\theta, \phi; n', m') \sin\theta d\theta = n(n+1)\delta_{nn'}\delta_{mm'}$$

$$\int_0^{2\pi} d\phi \int_0^{\pi} \boldsymbol{N}(\theta, \phi; n, m) \cdot \bar{\boldsymbol{N}}(\theta, \phi; n', m') \sin\theta d\theta = n(n+1)\delta_{nn'}\delta_{mm'}, \tag{A7}$$

where a dot means scalar product. The expansion coefficients can be found, for instance, for the scalar function ψ and the elastic displacement vector $\boldsymbol{u}$, as

$$\Phi(r; n, m) = \int_0^{2\pi} d\phi \int_0^{\pi} \sin\theta d\theta[\psi(r, \theta, \phi)\bar{S}(\theta, \phi)]$$

$$U_L(r; n, m) = \int_0^{2\pi} d\phi \int_0^{\pi} \sin\theta d\theta[\boldsymbol{u}(r, \theta, \phi) \cdot \bar{\boldsymbol{L}}(\theta, \phi)]$$

$$U_M(r; n, m) = \frac{1}{n(n+1)} \int_0^{2\pi} d\phi \int_0^{\pi} \sin\theta d\theta[\boldsymbol{u}(r, \theta, \phi) \cdot \bar{\boldsymbol{M}}(\theta, \phi)]$$

$$U_N(r; n, m) = \frac{1}{n(n+1)} \int_0^{2\pi} d\phi \int_0^{\pi} \sin\theta d\theta[\boldsymbol{u}(r, \theta, \phi) \cdot \bar{\boldsymbol{N}}(\theta, \phi)]. \tag{A8}$$

APPENDIX B: MATRICES AND THEIR ELEMENTS IN EQ. (20b)

First, eq. (18) can be ordered as

$$[T] = \frac{1}{r}[R_1][U] + [R_2]\partial_r[U] \tag{B1}$$

$$\partial_r[T] = \frac{1}{r}[R_3][T] + \frac{1}{r^2}[R_4][U] + \frac{1}{r}[R_5]\partial_r[U], \tag{B2}$$

where

$$[R_1] = \begin{bmatrix} 2c_{13} & -n(n+1)c_{13} & 0 \\ c_{44} & -c_{44} & 0 \\ 4\pi G\bar{\rho}\bar{r} & 0 & n+1 \end{bmatrix}; \quad [R_2] = \begin{bmatrix} c_{33} & 0 & 0 \\ 0 & c_{44} & 0 \\ 0 & 0 & 1 \end{bmatrix} \tag{B3}$$

$$[R_3] = \begin{bmatrix} -2 & n(n+1) & 0 \\ 0 & -3 & 0 \\ 0 & 0 & 0 \end{bmatrix}; \quad [R_5] = \begin{bmatrix} 2c_{13} & 0 & \bar{\rho}\bar{r} \\ -c_{13} & 0 & 0 \\ 0 & 0 & n-1 \end{bmatrix} \tag{B4}$$

$$[R_4] = \begin{bmatrix} 2(c_{11}+c_{12}) - 4g\bar{\rho}\bar{r} + 4\pi G(\bar{\rho}\bar{r})^2 & n(n+1)g\bar{\rho}\bar{r} - (c_{11}+c_{12})n(n+1) & 0 \\ g\bar{\rho}\bar{r} - (c_{11}+c_{12}) & c_{12}n(n+1) - 2c_{66}[1-n(n+1)] & \bar{\rho}\bar{r} \\ -8\pi G\bar{\rho}\bar{r} & 4\pi G\bar{\rho}\bar{r}n(n+1) & (n+1)(n-1) \end{bmatrix}.$$

For the given layer, we introduce the variable transformation as defined by eq. (19). Then, in terms of the new variable ξ, eqs (B1) and (B2) can be recast into

$$r(\xi)[T] = [R_1][U] + [R_2]\partial_\xi[U] \tag{B5}$$

$$r(\xi)\partial_\xi[T] = r(\xi)[R_3][T] + [R_4][U] + [R_5]\partial_\xi[U]. \tag{B6}$$

Eqs (B5) and (B6) can be combined and presented in the following enlarged matrix form

$$\begin{bmatrix} R_2 & 0 \\ -R_5 & I \end{bmatrix}\begin{bmatrix} U' \\ rT' \end{bmatrix} = \begin{bmatrix} -R_1 & I \\ R_4 & R_3 \end{bmatrix}\begin{bmatrix} U \\ rT \end{bmatrix}, \tag{B7}$$

where the superscript prime denotes derivative with respect to ξ.

APPENDIX C: THE PERTURBED POTENTIAL AND LOAD LOVE NUMBERS

C1. Boundary conditions of the traction and the perturbed gravitational potential

We introduce the total potential Ψ as

$$\Psi = \psi_0 + \psi, \tag{C1}$$

where ψ_0 is the potential before the perturbation, and therefore it satisfies the following governing equations and boundary conditions

$$\psi_{0,kk} \equiv \partial_r^2\psi_0 + \frac{2}{r}\partial_r\psi_0 = \begin{cases} -4\pi G\rho(r) & r < a \\ 0 & r > a \end{cases} \tag{C2}$$

$$\psi_0^{(i)} = \psi_0^{(e)}; \quad \partial_r\psi_0^{(i)} = \partial_r\psi_0^{(e)}; \quad r = a, \tag{C3}$$

where the superscripts (i) and (e) denote the internal $(r < a)$ and external $(r > a)$ quantities. On the deformed surface $r = a + u_r(a)$, we then have

$$\Psi^{(i)}(a + u_r) = \Psi^{(e)}(a + u_r); \quad \partial_r\Psi^{(i)}(a + u_r) - \partial_r\Psi^{(e)}(a + u_r) = -4\pi G\gamma, \tag{C4}$$

where γ (say $= \rho_w h_w$ with ρ_w being the ocean (water) density and h_w the ocean height of the water) is the mass applied on the surface of the Earth.

Making use of eqs (C1)–(C3) and in terms of the perturbed potential ψ, we have the following boundary conditions (by keeping only the first-degree small variables)

$$\psi^{(i)}(a) = \psi^{(e)}(a); \qquad \partial_r \psi^{(i)}(a) - \partial_r \psi^{(e)}(a) = -4\pi G(\rho u_r + \gamma). \tag{C5}$$

Now the perturbed gravitational potential ψ can be expressed in general as the summation of the following two terms:

$$\psi = \psi_d + \psi_l, \tag{C6}$$

where the subscripts d and l denote the deformation-perturbed potential and load potential (the potential related to the applied load).

C2. Deformation-related perturbed potential ψ_d

It is obvious that ψ_d should satisfy the following governing equations

$$\psi_{d,jj} = \begin{cases} -4\pi G(\rho u_{j,j} + \rho_{,r} u_r); & r < a \\ 0; & r > a \end{cases} \tag{C7}$$

and the condition on the surface of the Earth $r = a$

$$\psi_d^{(i)} = \psi_d^{(e)}; \qquad \partial_r \psi_d^{(i)} - \partial_r \psi_d^{(e)} = -4\pi G\rho u_r. \tag{C8}$$

From now on, our analysis will be restricted to the nth term of the spherical surface function S (i.e. any time n appears, it means the relation for the nth term). We notice that in $r > a$, ψ_d should satisfy the Laplace equation (the second expression in C7), that is it should be harmonic. Therefore, on the surface $r = a$, we have the following relation.

$$\partial_r \psi_d^{(e)} = -\frac{n+1}{a} \psi_d^{(e)}. \tag{C9}$$

Thus, the second expression in (C8) becomes ($r = a$)

$$\partial_r \psi_d^{(i)} + \frac{n+1}{a} \psi_d^{(i)} = -4\pi G\rho u_r. \tag{C10}$$

The right-hand side is also understood as the nth term of the radial displacement u_r. Using the relations among different potentials in eq. (C6), eq. (C10) becomes ($r = a$)

$$\partial_r \psi^{(i)} + \frac{n+1}{a} \psi^{(i)} = -4\pi G\rho u_r + \frac{2n+1}{a} \psi_l. \tag{C11}$$

On the right-hand side of eq. (C11), the load potential can be either from inside or outside of the Earth since it is continuous at $r = a$. Furthermore, it is noted that the nth term of ψ_l is proportional to S_n as

$$\psi_l \propto \frac{r^n}{a^n} S_n, \tag{C12}$$

where $S_n = S(\theta, \phi; n, m)$ is the nth spherical function. Therefore, in terms of the expansion coefficients, eq. (C11) can be finally expressed on the surface $r = a$ as

$$Q(a) = \frac{2n+1}{a} \psi_l. \tag{C13}$$

The right-hand side is understood as the expansion coefficient of the nth term.

Therefore, for the surface loading case, the traction and potential flux boundary conditions on the surface of $r = a$ become (their expansion coefficients)

$$T_L(a) = -g_a \gamma; \quad T_M(a) = 0; \qquad Q(a) = \frac{2n+1}{a} \psi_l. \tag{C14}$$

Using the mass expansion coefficients, we have

$$T_L(a) = -g_a C_n^m; \quad T_M(a) = 0; \qquad Q(a) = -4\pi G C_n^m, \tag{C15}$$

where we have assumed that the scalar mass γ can be expanded as (the expansion coefficients should be also a function of time t)

$$\gamma(\theta, \phi) = \sum_{n=0}^{\infty} \sum_{m=-n}^{n} C_n^m S(\theta, \phi). \tag{C16}$$

The load-related perturbed potential ψ_l can be expanded as

$$\psi_l(r, \theta, \phi) = \begin{cases} \sum_{n=0}^{N} \sum_{m=-n}^{n} A_n^m \frac{r^n}{a^n} S(\theta, \phi); & r < a \\ \sum_{n=0}^{N} \sum_{m=-n}^{n} A_n^m \frac{a^{n+1}}{r^{n+1}} S(\theta, \phi); & r > a \end{cases}, \tag{C17}$$

where it can be shown that

$$A_n^m = \frac{-4\pi G a}{2n+1} C_n^m. \tag{C18}$$

Or

$$\psi_l(r, \theta, \phi) = -\begin{cases} \sum_{n=0}^{N} \sum_{m=-n}^{n} \frac{4\pi G a}{2n+1} C_n^m \frac{r^n}{a^n} S(\theta, \phi); & r < a \\ \sum_{n=0}^{N} \sum_{m=-n}^{n} \frac{4\pi G a}{2n+1} C_n^m \frac{a^{n+1}}{r^{n+1}} S(\theta, \phi); & r > a \end{cases}. \tag{C19}$$

We now briefly derive the relation eq. (C18):

First, the load-related perturbed potential ψ_l should satisfy

$$\begin{cases} \partial_j \partial_j \psi_l^{(i)} = 0; & r < a \\ \partial_j \partial_j \psi_l^{(e)} = 0; & r > a \end{cases} \tag{C20}$$

with its solutions being

$$\psi_s^{(i)}(r, \theta, \phi) = \sum_{n=0}^{N} \sum_{m=-n}^{n} A_n^m \frac{r^n}{a^n} S(\theta, \phi); \quad r < a$$

$$\psi_s^{(e)}(r, \theta, \phi) = \sum_{n=0}^{N} \sum_{m=-n}^{n} A_n^m \frac{a^{n+1}}{r^{n+1}} S(\theta, \phi); \quad r > a. \tag{C21}$$

At $r = a$, the following conditions should be satisfied

$$\psi_s^{(i)} = \psi_s^{(e)}; \qquad \partial_r \psi_s^{(i)} - \partial_r \psi_s^{(e)} = -4\pi G \gamma. \tag{C22}$$

Then, substituting eqs (C16) and (C21) into eq. (C22) gives eq. (C18).

C3. Definition of LLNs

The three load Love numbers LLNs (h_n, l_n, k_n) on the surface of the Earth $r = a$ can be defined as (for the physical quantities proportional to the magnitude of the nth term of the harmonic surface load potential ψ_l)

$$u_r(a, \theta, \phi) = \frac{h_n}{g_a} \psi_l$$

$$u_\theta(a, \theta, \phi) = \frac{l_n}{g_a} \partial_\theta \psi_l$$

$$\psi_d(a, \theta, \phi) = k_n \psi_l. \tag{C23}$$

It is easy to see that (in terms of the magnitude of the expansion coefficients of ψ_l)

$$h_n = (2n+1)U_L(a)g_a/(4\pi GC_n^m);$$

$$l_n = (2n+1)U_M(a)g_a/(4\pi GC_n^m);$$

$$k_n = -[(2n+1)\Phi(a)g_a/(4\pi GC_n^m) + 1]. \tag{C24}$$

C4. Solutions and LLNs for degree $n = 1$

It is well known (Farrell 1972; Saito 1974; Pan *et al.* 1986) that when $n = 1$, there is a rigid-body motion solution in eq. (13) and this solution can be expressed as (with superscript r being rigid motion)

$$\mathbf{U}^r = [\,1 \quad 1 \quad g\,]^t; \quad \mathbf{T}^r = \mathbf{0}. \tag{C25}$$

Following Farrell (1972), we let any one of the coefficients c_i in eq. (38), say, $c_3 = 0$, and then propagate the solution matrices to the surface to satisfy any two of the three boundary conditions in eq. (38). We name the solution thus found as $\mathbf{U}^c$ and $\mathbf{T}^c$, and notice that it contains a rigid-body motion of the center of the Earth after loading. Since eq. (C25) is also a solution, it is obvious that the following expression also constitutes a new solution to the problem (with α being a coefficient to be determined)

$$\mathbf{U} = \mathbf{U}^c + \alpha\mathbf{U}^r; \quad \mathbf{T} = \mathbf{T}^c + \alpha\mathbf{T}^r. \tag{C26}$$

This equation actually provides us a condition to constrain the center of the Earth. If we assume that the deformed center of the Earth (CE) is fixed in the space, we then find that

$$\alpha = -\Phi^c(a)/g. \tag{C27}$$

The new LLNs are then obtained as

$$h_1 = h_1^c - k_1^c; \quad l_1 = l_1^c - k_1^c; \quad k_1 = 0, \tag{C28}$$

where the LLNs with superscript 'c' are those calculated based on the solution $\mathbf{U}^c$ and $\mathbf{T}^c$. We further point out that the LLNs with superscript 'c' in eq. (C28) are actually those based on the centre of mass (CM) reference system.

APPENDIX D: ANALYTICAL SOLUTIONS FOR DEGREE $n = 0$

When $n = 0$, we have only the spherical symmetric deformation. In other words, the solution depends only on the radial coordinate r. As such, the N-type and M-type coefficients should be all zero, and we are thus left with only the L-type expansion coefficients. For the governing equations without body force, we have in the mantle,

$$U_L' = -\frac{2c_{13}}{c_{33}}\frac{U_L}{r} + \frac{T_L}{c_{33}}$$

$$\Phi' = -4\pi G\rho U_L - \frac{1}{r}\Phi + Q$$

$$T_L' = -\frac{4\rho g U_L}{r} + \frac{2[c_{33}(c_{11}+c_{12}) - 2c_{13}^2]U_L}{c_{33}r^2} + \frac{2}{r}\left(\frac{c_{13}}{c_{33}} - 1\right)T_L - \frac{1}{r}\rho\Phi + \rho Q$$

$$Q' = -4\pi G\rho\frac{U_L}{r} - \frac{1}{r}Q. \tag{D1}$$

From the second and fourth expressions, we have

$$\frac{\Phi'}{r} + \frac{1}{r^2}\Phi = Q' + \frac{2}{r}Q. \tag{D2}$$

A solution of which is

$$Q = \frac{1}{r}\Phi. \tag{D3}$$

Eq. (D1) is therefore changed to

$$U'_L = -\frac{2c_{13}}{c_{33}}\frac{U_L}{r} + \frac{T_L}{c_{33}}$$

$$T'_L = -\frac{4\rho g U_L}{r} + \frac{2[c_{33}(c_{11}+c_{12}) - 2c_{13}^2]U_L}{c_{33}r^2} + \frac{2}{r}\left(\frac{c_{13}}{c_{33}} - 1\right)T_L$$

$$\Phi' = -4\pi G\rho U_L. \tag{D4}$$

Eq. (D4) indicates that the elastic spherical deformation is uncoupled from the perturbed gravitational potential and, therefore, can be solved independent of it. In other words, for degree $n = 0$, we need only to solve U_L and T_L using the first two expressions in eq. (D4), subjected to the following interface continuity conditions.

$$[U_L]_-^+ = 0; \quad [T_L]_-^+ = 0. \tag{D5}$$

Making use of the density assumption of $1/r$ in eq. (15), the first two expressions in eq. (D4) can be written as

$$U'_L = -\frac{2c_{13}}{c_{33}}\frac{U_L}{r} + \frac{T_L}{c_{33}}$$

$$T'_L = -\frac{4\bar\rho \bar r g U_L}{r^2} + \frac{2[c_{33}(c_{11}+c_{12}) - 2c_{13}^2]U_L}{c_{33}r^2} + \frac{2}{r}\left(\frac{c_{13}}{c_{33}} - 1\right)T_L. \tag{D6}$$

Eq. (D6) can be further written as

$$U'_L = b_{11}\frac{U_L}{r} + b_{12}T_L$$

$$T'_L = b_{21}\frac{U_L}{r^2} + b_{22}\frac{T_L}{r} \tag{D7}$$

with the coefficients b_{ij} being

$$b_{11} = -2c_{13}/c_{33}; \quad b_{12} = 1/c_{33}; \quad b_{22} = 2(c_{13}/c_{33} - 1)$$

$$b_{21} = -4\bar\rho \bar r g + 2[c_{33}(c_{11}+c_{12}) - 2c_{13}^2]/c_{33}, \tag{D8}$$

where the isotropic case can be reduced by using eq. (5).

Making use of the exponential variable transformation as defined by eq. (19), we can change eq. (D7) to

$$\begin{bmatrix} U'_L \\ rT'_L \end{bmatrix} = \begin{bmatrix} b_{11} & b_{12} \\ b_{21} & b_{22} \end{bmatrix}\begin{bmatrix} U_L \\ rT_L \end{bmatrix}, \tag{D9}$$

where the prime denotes the derivative with respect to variable ξ.

In terms of the exponential matrix, the general solution of eq. (D9) in the given layer at ξ can be expressed in terms of its solution at $\xi = 0$ as

$$\begin{bmatrix} U_L(\xi) \\ r(\xi)T_L(\xi) \end{bmatrix} = \exp(A\xi)\begin{bmatrix} U_L(0) \\ r(\xi)T_L(0) \end{bmatrix}, \tag{D10}$$

where matrix $[A]$ is related to b_{ij} as

$$[A] = \begin{bmatrix} b_{11} & b_{12} \\ b_{21} & b_{22} + 1 \end{bmatrix}. \tag{D11}$$

Relation (D10) can be propagated, in the mantle, from the core–mantle boundary $r = r_c$ to the surface at $r = a$ to obtain

$$\begin{bmatrix} U_L(\xi_p) \\ aT_L(\xi_p) \end{bmatrix}\Bigg|_{r=a} = \exp\left(A_p\xi_p\right)\exp\left(A_{p-1}\xi_{p-1}\right)\cdots\exp\left(A_1\xi_1\right)\begin{bmatrix} U_L(\xi) \\ r_cT_L(\xi) \end{bmatrix}\Bigg|_{r=r_c}, \tag{D12}$$

where matrix $[A_i]$ is related to the material properties in layer i as defined in eq. (D11).

In the core ($r < r_c$ which is isotropic with $\mu = 0$), the first two expressions in eq. (D4) are reduced to

$$U'_L = -\frac{2U_L}{r} + \frac{1}{\lambda}T_L; \qquad T'_L = -\frac{4\rho g U_L}{r}. \tag{D13}$$

Same as for the other degree n, we assume that the gravity in each layer of the core are linear, that is $g = kr$, and that the density is constant. Then we can rewrite eq. (D13) as

$$U'_L = -\frac{2U_L}{r} + \frac{T_L}{\lambda}; \qquad T'_L = -4\rho k U_L. \tag{D14}$$

The general solution of eq. (D14) can be expressed as

$$\begin{bmatrix} U_L \\ rT_L \end{bmatrix} = [\boldsymbol{B}] \begin{bmatrix} c_1 \\ c_2 \end{bmatrix} \tag{D15}$$

with the solution matrix $[\boldsymbol{B}]$ being

$$[\boldsymbol{B}(pr)] = \begin{bmatrix} j_1(pr) & y_1(pr) \\ \lambda[pr j'_1(pr) + 2j_1(pr)] & \lambda[pr y'_1(pr) + 2y_1(pr)] \end{bmatrix}. \tag{D16}$$

In eq. (D16), the prime denotes derivative with respect to the combined variable (pr), not with respect to r, and

$$p = \sqrt{4\rho k/\lambda}. \tag{D17}$$

Also in eq. (D16), j_1 and y_1 are the spherical Bessel functions of the first and second kinds.

As we pointed out in Section 4, instead of assuming $g = kr$ in each layer, one could assume that the density varies as $1/r$ in each layer. This will also lead us to the analytical solution associated with degree $n = 0$.

From the general solution eq. (D15), we have the following propagating relation between the upper and lower interfaces of layer i, as

$$\begin{bmatrix} U_L \\ r_i T_L \end{bmatrix} = [\boldsymbol{a}^c_i] \begin{bmatrix} U_L \\ r_{i-1} T_L \end{bmatrix}, \tag{D18}$$

where

$$[\boldsymbol{a}^c_i] = [\boldsymbol{B}(pr_i)][\boldsymbol{B}(pr_{i-1})]^{-1}. \tag{D19}$$

Thus, the propagating relation (D18) can be propagated from one layer to the next. What we need now is just the starting solution of eq. (D13) in the innermost core when r is very small. Since at the centre $r = 0$, we have $g = 0$ and $\rho = $ constant, we have, near the centre,

$$\lambda U'_L = -\frac{2\lambda U_L}{r} + T_L; \qquad T'_L = 0 \tag{D20}$$

which has a general solution when $r \leq r_0$ as

$$\begin{bmatrix} U_L \\ rT_L \end{bmatrix} = \begin{bmatrix} r \\ 3\lambda r \end{bmatrix} c. \tag{D21}$$

We therefore can propagate the solution from $r = r_0$ all the way to the surface at $r = a$ to obtain

$$\begin{bmatrix} U_L(\xi_p) \\ a T_L(\xi_p) \end{bmatrix} \bigg|_{r=a} = \exp\left(A_p \xi_p\right) \exp\left(A_{p-1}\xi_{p-1}\right) \cdots [\boldsymbol{a}^c_m][\boldsymbol{a}^c_{m-1}] \cdots [\boldsymbol{a}^c_1] \begin{bmatrix} r_0 \\ 3\lambda r_0 \end{bmatrix} c. \tag{D22}$$

Then, applying the surface condition

$$T_L(a) = -g_a C^0_0 \tag{D23}$$

to the second expression in eq. (D22), we can solve for the unknown constant c; substituting back to the first expression in eq. (D22), we find $U_L(a)$, and thus the only nonzero LLN for degree $n = 0$ as

$$h_0 = U_L(a) g_a / (4\pi G C^0_0). \tag{D24}$$

We point out that, for the incompressible mantle and core models (i.e. Model 4 with 56Inc-26Inc and Model 5 with 56Inc-UInc), the solutions of U_L and T_L in each layer are zero and therefore, the LLN $h_0 = 0$ (Longman 1963; Farrell 1972; Pan *et al.* 1986). For other models discussed in this paper, we have $h_0 = -0.13431$ for the transversely isotropic Model 1 (56CT-26C), $h_0 = -0.13396$ for the isotropic Model 2 (56C-26C), and $h_0 = -0.10811$ for the isotropic Model 3 (56C-UInc).

APPENDIX E: BENCHMARK MODEL OF SPADA *ET AL.* (2011)

Table E1. Benchmark model of Spada *et al.* (2011).

Layer #	Radius r_i (m)	Density (kg m^{-3})	μ (Pa)	Gravity (m s^{-2})
5	6 371 000	3037	5.0605E10	9.83479662
4	6 301 000	3438	7.0363E10	9.90985890
3	5 951 000	3871	1.0549E11	9.99820846
2	5 701 000	4978	2.2834E11	9.81493357
1	3 480 000	10 750	2.2834E11	10.45700000

Notes. The gravity in our model is the average in the layer calculated using eq. (17) with the input density satisfying eq. (15). Therefore, while Spada *et al.* (2011) used constant density and varying gravity from the Newton's law, we used $1/r$-density variation as described by eq. (15) and constant gravity which is the average in the layer calculated using eq. (17).

APPENDIX F: PREM MODELS OF LAYERED MANTLE AND CORE

Table F1. Mantle Model TI56 (layered compressible and transversely isotropic mantle).

Layer #	Radius r_i (m)	Density (kg m^{-3})	A (Pa)	C (Pa)	L (Pa)	N (Pa)	F (Pa)	Gravity (m s^{-2})
57	6 371 000	2600	8.746667E10	8.746667E10	2.660000E10	2.660000E10	3.426667E10	9.8156
56	6 369 000	2600	8.750000E10	8.750000E10	2.660000E10	2.660000E10	3.430000E10	9.8222
55	6 356 000	2900	1.341000E11	1.341000E11	4.410000E10	4.410000E10	4.590000E10	9.8332
54	6 346 600	3380	2.268000E11	2.176000E11	6.530000E10	7.190000E10	8.660000E10	9.8394
53	6 331 000	3378	2.260000E11	2.165000E11	6.540000E10	7.140000E10	8.630000E10	9.8437
52	6 311 000	3376	2.251000E11	2.151000E11	6.550000E10	7.080000E10	8.600000E10	9.8493
51	6 291 000	3372	2.237714E11	2.132000E11	6.564286E10	6.994286E10	8.557143E10	9.8553
50	6 256 000	3369	2.221429E11	2.108857E11	6.581429E10	6.894286E10	8.502857E10	9.8664
49	6 221 000	3365	2.205286E11	2.085857E11	6.598571E10	6.798571E10	8.435714E10	9.8783
48	6 186 000	3356	2.189857E11	2.063000E11	6.615714E10	6.695714E10	8.367143E10	9.8911
47	6 151 000	3449	2.517000E11	2.517000E11	7.410000E10	7.410000E10	1.035000E11	9.9048
46	6 106 000	3476	2.588333E11	2.588333E11	7.570000E10	7.570000E10	1.074333E11	9.9203
45	6 061 000	3503	2.660667E11	2.660667E11	7.730000E10	7.730000E10	1.114667E11	9.9361
44	6 016 000	3530	2.735333E11	2.735333E11	7.900000E10	7.900000E10	1.155333E11	9.9522
43	5 971 000	3755	3.107000E11	3.107000E11	9.060000E10	9.060000E10	1.295000E11	9.9686
42	5 921 000	3818	3.339667E11	3.339667E11	9.770000E10	9.770000E10	1.385667E11	9.979
41	5 871 000	3881	3.582333E11	3.582333E11	1.051000E11	1.051000E11	1.480333E11	9.9883
40	5 821 000	3944	3.836000E11	3.836000E11	1.128000E11	1.128000E11	1.580000E11	9.9965
39	5 771 000	3980	4.102333E11	4.102333E11	1.210000E11	1.210000E11	1.682333E11	10.0038
38	5 736 000	3988	4.155000E11	4.155000E11	1.224000E11	1.224000E11	1.707000E11	10.0088
37	5 701 000	4397	5.063000E11	5.063000E11	1.548000E11	1.548000E11	1.967000E11	10.0143
36	5 650 000	4428	5.252333E11	5.252333E11	1.639000E11	1.639000E11	1.974333E11	10.0063
35	5 600 000	4474	5.439667E11	5.439667E11	1.730000E11	1.730000E11	1.979667E11	9.9985
34	5 500 000	4534	5.695000E11	5.695000E11	1.794000E11	1.794000E11	2.107000E11	9.9836
33	5 400 000	4592	5.945667E11	5.945667E11	1.856000E11	1.856000E11	2.233667E11	9.9698
32	5 300 000	4650	6.195333E11	6.195333E11	1.918000E11	1.918000E11	2.359333E11	9.9573
31	5 200 000	4707	6.441667E11	6.441667E11	1.979000E11	1.979000E11	2.483667E11	9.9467
30	5 100 000	4762	6.684667E11	6.684667E11	2.039000E11	2.039000E11	2.606667E11	9.9383
29	5 000 000	4817	6.925333E11	6.925333E11	2.098000E11	2.098000E11	2.729333E11	9.9326
28	4 900 000	4871	7.164000E11	7.164000E11	2.157000E11	2.157000E11	2.850000E11	9.9301
27	4 800 000	4924	7.401333E11	7.401333E11	2.215000E11	2.215000E11	2.971333E11	9.9314
26	4 700 000	4964	7.637667E11	7.637667E11	2.273000E11	2.273000E11	3.091667E11	9.9369
25	4 650 000	4990	7.637667E11	7.637667E11	2.273000E11	2.273000E11	3.091667E11	9.9369
24	4 600 000	5022	7.874000E11	7.874000E11	2.331000E11	2.331000E11	3.212000E11	9.9474
23	4 550 000	5042	7.874000E11	7.874000E11	2.331000E11	2.331000E11	3.212000E11	9.9474
22	4 500 000	5068	8.109000E11	8.109000E11	2.388000E11	2.388000E11	3.333000E11	9.9635
21	4 450 000	5093	8.109000E11	8.109000E11	2.388000E11	2.388000E11	3.333000E11	9.9635
20	4 400 000	5119	8.345000E11	8.345000E11	2.445000E11	2.445000E11	3.455000E11	9.9859
19	4 350 000	5144	8.345000E11	8.345000E11	2.445000E11	2.445000E11	3.455000E11	9.9859
18	4 300 000	5169	8.582000E11	8.582000E11	2.502000E11	2.502000E11	3.578000E11	10.0156
17	4 250 000	5195	8.582000E11	8.582000E11	2.502000E11	2.502000E11	3.578000E11	10.0156

Table F1 *Continued.*

Layer #	Radius r_i (m)	Density (kg m^{-3})	A (Pa)	C (Pa)	L (Pa)	N (Pa)	F (Pa)	Gravity (m s^{-2})
16	4 200 000	5220	8.821000E11	8.821000E11	2.559000E11	2.559000E11	3.703000E11	10.0535
15	4 150 000	5245	8.821000E11	8.821000E11	2.559000E11	2.559000E11	3.703000E11	10.0535
14	4 100 000	5270	9.064333E11	9.064333E11	2.617000E11	2.617000E11	3.830333E11	10.1006
13	4 050 000	5295	9.064333E11	9.064333E11	2.617000E11	2.617000E11	3.830333E11	10.1006
12	4 000 000	5320	9.310667E11	9.310667E11	2.675000E11	2.675000E11	3.960667E11	10.158
11	3 950 000	5345	9.310667E11	9.310667E11	2.675000E11	2.675000E11	3.960667E11	10.158
10	3 900 000	5370	9.562333E11	9.562333E11	2.734000E11	2.734000E11	4.094333E11	10.2272
9	3 850 000	5394	9.562333E11	9.562333E11	2.734000E11	2.734000E11	4.094333E11	10.2272
8	3 800 000	5419	9.820333E11	9.820333E11	2.794000E11	2.794000E11	4.232333E11	10.3095
7	3 750 000	5444	9.820333E11	9.820333E11	2.794000E11	2.794000E11	4.232333E11	10.3095
6	3 700 000	5474	1.008567E12	1.008567E12	2.855000E11	2.855000E11	4.375667E11	10.4066
5	3 630 000	5499	1.027733E12	1.027733E12	2.899000E11	2.899000E11	4.479333E11	10.4844
4	3 600 000	5519	1.031600E12	1.031600E12	2.907000E11	2.907000E11	4.502000E11	10.5204
3	3 550 000	5544	1.031600E12	1.031600E12	2.907000E11	2.907000E11	4.502000E11	10.5204
2	3 500 000	5561	1.044767E12	1.044767E12	2.933000E11	2.933000E11	4.581667E11	10.6532
1	3 480 000	10932	9.420000E11	9.420000E11	0.000000E00	0.000000E00	9.420000E11	10.6823

Table F2. Mantle Model 56 (layered compressible and isotropic mantle).

Layer #	Radius r_i (m)	Density (kg m^{-3})	μ (Pa)	λ (Pa)	Gravity (m s^{-2})
57	6 371 000	2600	2.660000E10	3.426667E10	9.8156
56	6 369 000	2600	2.660000E10	3.430000E10	9.8222
55	6 356 000	2900	4.410000E10	4.590000E10	9.8332
54	6 346 600	3380	6.820000E10	8.603333E10	9.8394
53	6 331 000	3378	6.800000E10	8.576667E10	9.8437
52	6 311 000	3376	6.770000E10	8.556667E10	9.8493
51	6 291 000	3372	6.740000E10	8.536667E10	9.8553
50	6 256 000	3369	6.690000E10	8.490000E10	9.8664
49	6 221 000	3365	6.650000E10	8.436667E10	9.8783
48	6 186 000	3356	6.600000E10	8.380000E10	9.8911
47	6 151 000	3449	7.410000E10	1.035000E11	9.9048
46	6 106 000	3476	7.570000E10	1.074333E11	9.9203
45	6 061 000	3503	7.730000E10	1.114667E11	9.9361
44	6 016 000	3530	7.900000E10	1.155333E11	9.9522
43	5 971 000	3755	9.060000E10	1.295000E11	9.9686
42	5 921 000	3818	9.770000E10	1.385667E11	9.979
41	5 871 000	3881	1.051000E11	1.480333E11	9.9883
40	5 821 000	3944	1.128000E11	1.580000E11	9.9965
39	5 771 000	3980	1.210000E11	1.682333E11	10.0038
38	5 736 000	3988	1.224000E11	1.707000E11	10.0088
37	5 701 000	4397	1.548000E11	1.967000E11	10.0143
36	5 650 000	4428	1.639000E11	1.974333E11	10.0063
35	5 600 000	4474	1.730000E11	1.979667E11	9.9985
34	5 500 000	4534	1.794000E11	2.107000E11	9.9836
33	5 400 000	4592	1.856000E11	2.233667E11	9.9698
32	5 300 000	4650	1.918000E11	2.359333E11	9.9573
31	5 200 000	4707	1.979000E11	2.483667E11	9.9467
30	5 100 000	4762	2.039000E11	2.606667E11	9.9383
29	5 000 000	4817	2.098000E11	2.729333E11	9.9326
28	4 900 000	4871	2.157000E11	2.850000E11	9.9301
27	4 800 000	4924	2.215000E11	2.971333E11	9.9314
26	4 700 000	4964	2.273000E11	3.091667E11	9.9369
25	4 650 000	4990	2.273000E11	3.091667E11	9.9369
24	4 600 000	5022	2.331000E11	3.212000E11	9.9474
23	4 550 000	5042	2.331000E11	3.212000E11	9.9474
22	4 500 000	5068	2.388000E11	3.333000E11	9.9635

Table F2 *Continued.*

Layer #	Radius r_i (m)	Density (kg m^{-3})	μ (Pa)	λ (Pa)	Gravity (m s^{-2})
21	4 450 000	5093	2.388000E11	3.333000E11	9.9635
20	4 400 000	5119	2.445000E11	3.455000E11	9.9859
19	4 350 000	5144	2.445000E11	3.455000E11	9.9859
18	4 300 000	5169	2.502000E11	3.578000E11	10.0156
17	4 250 000	5195	2.502000E11	3.578000E11	10.0156
16	4 200 000	5220	2.559000E11	3.703000E11	10.0535
15	4 150 000	5245	2.559000E11	3.703000E11	10.0535
14	4 100 000	5270	2.617000E11	3.830333E11	10.1006
13	4 050 000	5295	2.617000E11	3.830333E11	10.1006
12	4 000 000	5320	2.675000E11	3.960667E11	10.158
11	3 950 000	5345	2.675000E11	3.960667E11	10.158
10	3 900 000	5370	2.734000E11	4.094333E11	10.2272
9	3 850 000	5394	2.734000E11	4.094333E11	10.2272
8	3 800 000	5419	2.794000E11	4.232333E11	10.3095
7	3 750 000	5444	2.794000E11	4.232333E11	10.3095
6	3 700 000	5474	2.855000E11	4.375667E11	10.4066
5	3 630 000	5499	2.899000E11	4.479333E11	10.4844
4	3 600 000	5519	2.907000E11	4.502000E11	10.5204
3	3 550 000	5544	2.907000E11	4.502000E11	10.5204
2	3 500 000	5561	2.933000E11	4.581667E11	10.6532
1	3 480 000	10932	0.000000E00	9.422500E11	10.6823

Table F3. Core Model 26 (layered compressible core).

Layer #	Radius r_i (m)	Density (kg m^{-3})	λ (Pa)	μ (Pa)	$k = g/r$ (1 s^{-2})
1	300 000	13082	1.4203E12	0	3.657114E-6
2	600 000	13042.8	1.4053E12	0	3.647526E-6
3	900 000	12964.4	1.3805E12	0	3.631139E-6
4	1 221 500	12841.6	1.3434E12	0	3.606401E-6
5	1 300 000	12145.8	1.2888E12	0	3.570438E-6
6	1 400 000	12097.4	1.2679E12	0	3.532848E-6
7	1 500 000	12039.9	1.2464E12	0	3.501614E-6
8	1 600 000	11978.7	1.2242E12	0	3.474695E-6
9	1 700 000	11913.7	1.2013E12	0	3.450718E-6
10	1 800 000	11844.8	1.1775E12	0	3.428741E-6
11	1 900 000	11771.9	1.1529E12	0	3.408098E-6
12	2 000 000	11694.7	1.1273E12	0	3.388300E-6
13	2 100 000	11613.4	1.1009E12	0	3.369001E-6
14	2 200 000	11527.5	1.0735E12	0	3.349924E-6
15	2 300 000	11437.2	1.0451E12	0	3.330871E-6
16	2 400 000	11342.1	1.0158E12	0	3.311674E-6
17	2 500 000	11242.2	9.8550E11	0	3.292208E-6
18	2 600 000	11137.4	9.5420E11	0	3.272370E-6
19	2 700 000	11027.6	9.2200E11	0	3.252078E-6
20	2 800 000	10912.5	8.8890E11	0	3.231255E-6
21	2 900 000	10792.1	8.5500E11	0	3.209843E-6
22	3 000 000	10666.3	8.2020E11	0	3.187790E-6
23	3 100 000	10534.9	7.8460E11	0	3.165050E-6
24	3 200 000	10397.8	7.4840E11	0	3.141582E-6
25	3 300 000	10254.8	7.1160E11	0	3.117348E-6
26	3 400 000	10105.9	6.7430E11	0	3.092315E-6
27	3 480 000	9966.76	6.4410E11	0	3.071688E-6

APPENDIX G: ASYMPTOTIC EXPRESSIONS FOR LLNs OF LARGE DEGREE *n*

When either using an analytic expression or solving the equations numerically, it is inevitable that one is to encounter numerical precision problems (Riva & Vermeersen 2002). These problems may occurs depending on specific implementation details (intrinsic precision of the tools/programming language/library used, choice of the algorithm, and many other minor aspects that may have a large impact), and thus it can be useful to have some asymptotic formulas which can also be used to check if the code behaves correctly.

　　We therefore provide some asymptotic expressions and show how they can be applied to the models studied in this paper. There are already published formulas (i.e. Guo *et al.* 2004), but they are not so accurate, therefore we provide our expressions for interested readers.

When calculating the LLNs for the different PREM models studied in this paper, we observed that, after certain large $n = N$, the asymptotic behaviours of the three LLNs can be approximately predicted using the following formulations (i.e. for any $n \geq N$)

$$-h_n = -h_\infty + \frac{a_1}{\log(n)} + \frac{a_2}{n^{a_3}};$$

$$nl_n = L_\infty + \frac{b_1}{\log(n)} + \frac{b_2}{n^{b_3}};$$

$$-nk_n = -K_\infty + \frac{c_1}{\log(n)} + \frac{c_2}{n^{c_3}}, \tag{G1}$$

where a_i, b_i and c_i are parameters to be determined, and h_∞, L_∞ and K_∞ are the limiting values of h_n, nl_n and nk_n at $n = \infty$. These limiting values correspond to the normalized surface responses in a layered half space under surface loading (e.g. Pan 1989). For the different PREM earth models studied in this paper, the homogeneous half-space solution associated with the Boussinesq problem can be utilized to calculate the limiting values (Farrell 1972)

$$\begin{bmatrix} -h_\infty \\ L_\infty \\ -K_\infty \end{bmatrix} = \frac{g_a m_e}{4\pi a^2(\lambda + \mu)} \begin{bmatrix} \frac{\lambda+2\mu}{\mu} \\ 1 \\ \frac{3\rho(\lambda+\mu)}{2\rho_e\mu} \end{bmatrix}, \tag{G2}$$

where m_e is the total mass of the Earth, ρ_e is the average density of the Earth, g_a the gravity on the surface, a again the radius of the Earth, ρ is the density, and λ and μ are the two Lame's constants in the surface layer of the Earth.

Taking Models 2 (56C-26C) and 5 (56Inc-UInc) as examples, we find that, respectively,

$$\begin{bmatrix} -h_\infty \\ L_\infty \\ -K_\infty \end{bmatrix} = \begin{bmatrix} 6.20964 \\ 1.88773 \\ 3.05623 \end{bmatrix} \tag{G3a}$$

$$\begin{bmatrix} -h_\infty \\ L_\infty \\ -K_\infty \end{bmatrix} = \begin{bmatrix} 4.32191 \\ 0 \\ 3.05623 \end{bmatrix}. \tag{G3b}$$

If we fix a_3, b_3 and c_3 at 2, and use only two points to find the remaining coefficients a_i, b_i and c_i ($i = 1, 2$) in each expression of eq. (G1), say using values at points $n = 5500$ and 6000, we found that eq. (G1) can be used to predict the LLNs for all $n > 6000$ with a relative error at most 0.001 per cent. The coefficients corresponding to these two models are listed below (obtained using Mathematica):

For Model 2 (56C-26C):

$$h_n : a_1 = -0.015898347743655127; \qquad a_2 = -14014.434029657581;$$

$$nl_n : b_1 = -0.0008892094449262606; \quad b_2 = 956.0053208811127;$$

$$nk_n : c_1 = -0.004181394183215393; \quad c_2 = -34213.31190196148. \tag{G4a}$$

For Model 5 (56Inc-UInc):

$$h_n : a_1 = -0.017903965270320094; \qquad a_2 = -37492.68804378623;$$

$$nl_n : b_1 = -0.0022483867448176258; \quad b_2 = -17415.994856316163;$$

$$nk_n : c_1 = -0.005112601693189441; \qquad c_2 = -41508.649287599255. \tag{G4b}$$

We now apply these asymptotic expressions for large degree n. While Fig. G1 shows the LLNs for Model 2 (56C-26C). Fig. G2 shows those for Model 5 (56Inc-UInc) where the LLNs are plotted for n from 1 to 100 000. It is noted that LLNs for any large n can be predicted based on eq. (G1). Furthermore, we have listed in Tables G1 and G2 some LLNs, respectively, for Model 2 (56C-26C) and Model 5 (56Inc-UInc) based on both direct calculation and asymptotic prediction of eq. (G1). It can be observed from these tables that the asymptotic prediction of the LLNs (in parentheses) based on eq. (G1) is very accurate in the entire range from $n = 3000$ to infinity, much better than other asymptotic expressions available in the literature.

We further point out that eq. (G1) is valid for $n > 6000$ only for the PREM models studied in this paper. For different mantle models with different thickness layers, the asymptotic behaviour needs to be carefully analysed for accuracy.
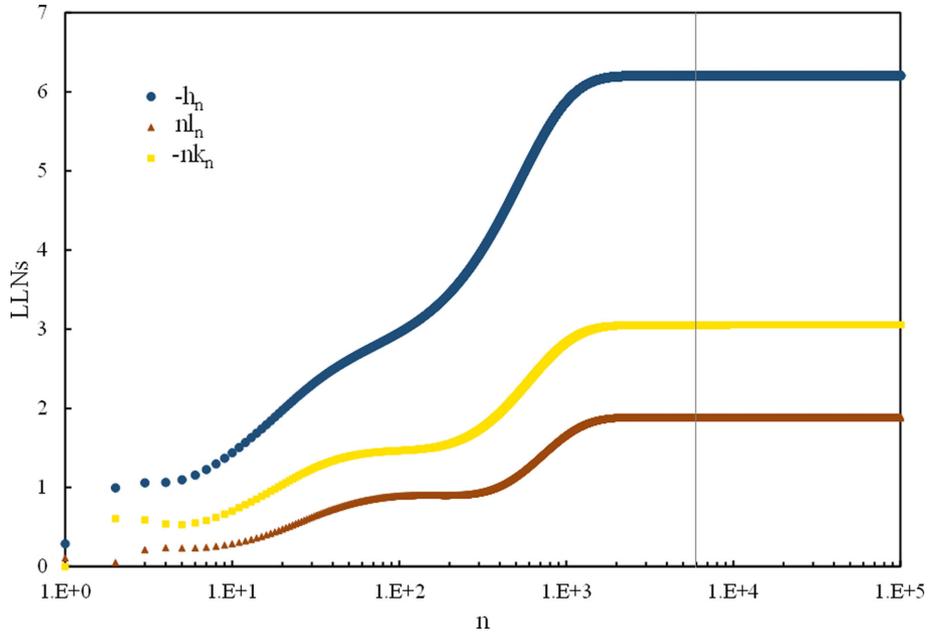
Figure G1. LLNs of Model 2 (56C-26C) versus *n* from 1 to 100 000 (analytical solution for $n \leq 6000$ and asymptotic solution (G1) for $n \geq 6000$).
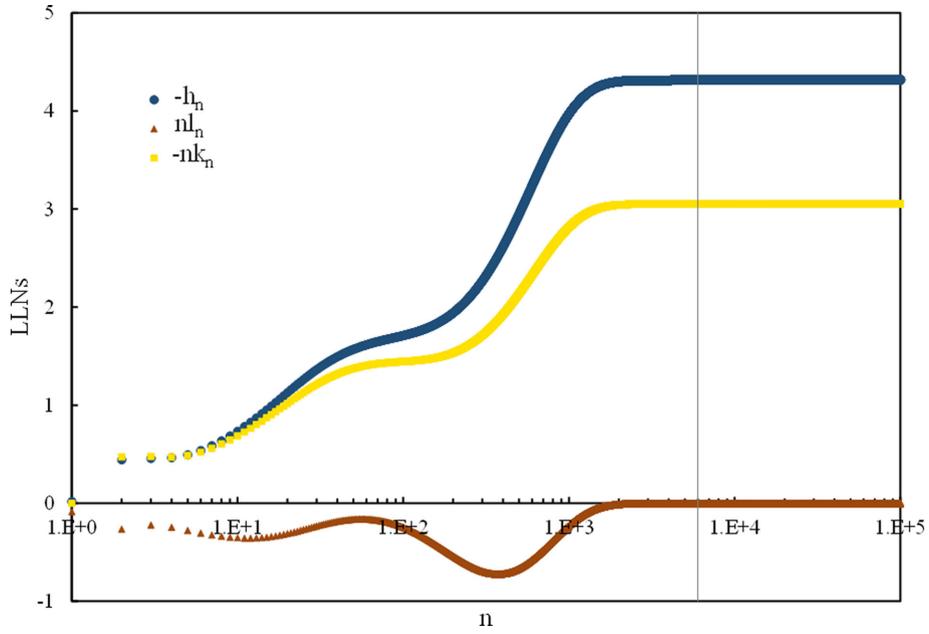

Figure G2. LLNs of Model 5 (56Inc-UInc) versus *n* from 1 to 100 000 (analytical solution for $n \leq 6000$ and asymptotic solution (G1) for $n \geq 6000$).

Table G1. LLNs ($-h_n$, nl_n and $-nk_n$) of the Earth Model 2 (56C-26C) for large n. Values without parentheses are directly calculated using our analytical formulations and those in parentheses are predicted based on the asymptotic expression eq. (G1).

n	$-h_n$	nl_n	$-nk_n$
3000	6.20355810 (6.20350857)	1.88737087 (1.88758049)	3.05190534 (3.05122818)
4000	6.20438579 (6.20434842)	1.88752214 (1.88754289)	3.05308800 (3.05293303)
4500	6.20460800 (6.20459405)	1.88752560 (1.88753381)	3.05345564 (3.05339807)
5000	6.20478282 (6.20477938)	1.88752552 (1.88752785)	3.05374779 (3.05373325)
5500	6.20492423 (6.20492423)	1.88752387 (1.88752387)	3.05398327 (3.05398327)
6000	6.20504074 (6.20504074)	1.88752120 (1.88752120)	3.05417510 (3.05417510)
6500	6.20513845 (6.20513669)	1.88751794 (1.88751942)	3.05433279 (3.05432578)
7000	6.20522158 (6.20521729)	1.88751427 (1.88751825)	3.05446373 (3.05444651)
7500	(6.20528612)	(1.88751753)	(3.05454491)
8000	(6.20534575)	(1.88751712)	(3.05462631)
10 000	(6.20552327)	(1.88751726)	(3.05484472)
20 000	(6.20590656)	(1.88752565)	(3.05517448)
50 000	(6.20624903)	(1.88754115)	(3.05532866)
100 000	(6.20645693)	(1.88755225)	(3.05539250)

Table G2. LLNs ($-h_n$, nl_n and $-nk_n$) of the Earth Model 5 (56Inc-UInc) for large n. Values without parentheses are directly calculated using our analytical formulations and those in parentheses are predicted based on the asymptotic expression eq. (G1).

n	$-h_n$	nl_n	$-nk_n$
3000	4.31324704 (4.31259147)	−0.00230948(−0.00258173)	3.05099448 (3.05014757)
4000	4.31477172 (4.31459263)	−0.00162003 (−0.00171269)	3.05241101 (3.05221635)
4500	4.31522456 (4.31515403)	−0.00143836 (−0.00147550)	3.05285395 (3.05278071)
5000	4.31558529 (4.31556644)	−0.00129445 (−0.00130448)	3.05320620 (3.05318749)
5500	4.31588028 (4.31588028)	−0.00117685 (−0.00117685)	3.05349094 (3.05349094)
6000	4.31612612 (4.31612612)	−0.00107888 (−0.00107888)	3.05372378 (3.05372378)
6500	4.31633422 (4.31632699)	−0.00099602 (−0.00100189)	3.05391629 (3.05390668)
7000	4.31651252 (4.31648853)	−0.00092478 (−0.00094017)	3.05407698 (3.05405324)
7500	(4.31662316)	(−0.00088984)	(3.05417271)
8000	(4.31673705)	(−0.00084818)	(3.05427154)
10 000	(4.31705908)	(−0.00073626)	(3.05453676)
20 000	(4.31765355)	(−0.00056630)	(3.05493754)
50 000	(4.31808481)	(−0.00048545)	(3.05512537)
100 000	(4.31832546)	(−0.00045142)	(3.05520333)